Swarm and Evolutionary Computation 78 (2023) 101290

Contents lists available at ScienceDirect

Swarm and Evolutionary Computation

journal homepage: www.elsevier.com/locate/swevo

Designing problem-specific operators for solving the Cell Switch-Off problem in ultra-dense 5G networks with hybrid MOEAs

Jesús Galeano-Brajones [a], Francisco Luna-Valero [b,c,*], Javier Carmona-Murillo [a], Pablo H. Zapata Cano [d], Juan F. Valenzuela-Valdés [e]

[a] Dpto. de Ingeniería de Sistemas Informáticos y Telemáticos, Universidad de Extremadura, Centro Universitario de Mérida, Mérida, 06800, Spain
[b] ITIS Software, Universidad de Málaga, Edificio de Investigación Ada Byron, Málaga, 29071, Spain
[c] Dpto. de Lenguajes y Ciencias de la Computación, Universidad de Málaga, E.T.S.I. Informática, Málaga, 29071, Spain
[d] School of Electrical and Computer Engineering, Aristotle University of Thessaloniki, Thessaloniki, 541 24, Greece
[e] Dpto. de Teoría de la Señal, Telemática y Comunicaciones, CITIC, Universidad de Granada, Granada, 18014, Spain

ARTICLE INFO

Dataset link: https://github.com/galeanobra/CSO_Hybrid, https://doi.org/10.6084/m9.figshare.21378000

Keywords:
Problem-specific operators
Hybridization
Multi-objective optimization
Ultra-dense networks
5G

ABSTRACT

The massive deployment of base stations is one of the key pillars of the fifth generation (5G) of mobile communications. However, this network densification entails high energy consumption that must be addressed to enhance the sustainability of this industry. This work faces this problem from a multi-objective optimization perspective, in which both energy efficiency and quality of service criteria are taken into account. To do so, several newly problem-specific operators have been designed so as to engineer hybrid multi-objective evolutionary metaheuristics (MOEAs) that bring expert knowledge of the domain to the search of the algorithms. These hybrid approaches have been able to improve upon canonical versions of the algorithms, clearly showing the contributions of our approach. Furthermore, this paper tests the hypothesis that the hybridization using several of those problem-specific operators simultaneously can enhance the search of MOEAs that are endowed only with a single one.

1. Introduction

Global mobile data traffic has increased massively, specially in the last decade, growing by 40% between Q1 2021 and Q1 2022. The high data transmission rates, along with other services that require ultra-low latency and reliable connections (e.g., autonomous driving, factory automation, etc.) or a massive number of narrowband Internet access (e.g., sensing and monitoring, Internet of Things, etc.), has promoted the development of a new generation of mobile communication systems, the fifth or 5G, to cope with such demanding scenarios and is currently under deployment. Indeed, 5G mobile subscriptions will surpass 1 billion in 2022, and are predicted to be 4.4 billion by the end of 2027, accounting for 48 percent of all mobile subscriptions [1]. 5G networks are expected to provide data rates 13 times higher than the average mobile connection by 2023, reaching 575 Mbps [2], as well as latencies below 1 ms and the support of more than one million devices per km^2. But this high performance must be achieved by saving 90% of power consumption, to make these new communication systems sustainable [3].

Three main paradigms have been identified to approach the challenging design requirements and expected performance indicators of 5G networks [4,5]: (i) using the millimeter wave (mmWave) spectrum to enable larger bandwidths, (ii) increasing spectral efficiency by multi-antenna transmission (massive, collaborative MIMO), and (iii) also increasing spatial reuse through network densification [6] both in horizontal (streets, hotspots, etc.) and vertical dimensions of the network (apartments, offices, etc.) [7]. The bandwidth requirements of 5G networks force switching to mmWave spectrum, with carrier frequencies of 30–300 GHz [8]. In these bands, many antennas are needed to overcome the path losses [9]. The combination of both massive MIMO and mmWave in a single technology mixes the prospects of having a large mmWave bandwidth available and the gains provided by massive MIMO antenna arrays. Thus, enabling access to the 30–300 GHz bands will substantially improve the spectral efficiency [10,11]. Furthermore, this reinforces the necessity of having an Ultra-Dense Network (UDN), since transmitting at higher frequencies requires a reduction of the user-antenna distance, which translates into a smaller cell size, in order to overcome channel difficulties like blocking and path-loss [12]. This work aims at reducing the impact of these last two paradigms on the energy consumption of 5G networks.

* Corresponding author at: Dpto. de Lenguajes y Ciencias de la Computación, Universidad de Málaga, E.T.S.I. Informática, Málaga, 29071, Spain.
E-mail address: flv@lcc.uma.es (F. Luna-Valero).

https://doi.org/10.1016/j.swevo.2023.101290
Received 21 October 2022; Received in revised form 4 January 2023; Accepted 3 March 2023
Available online 16 March 2023

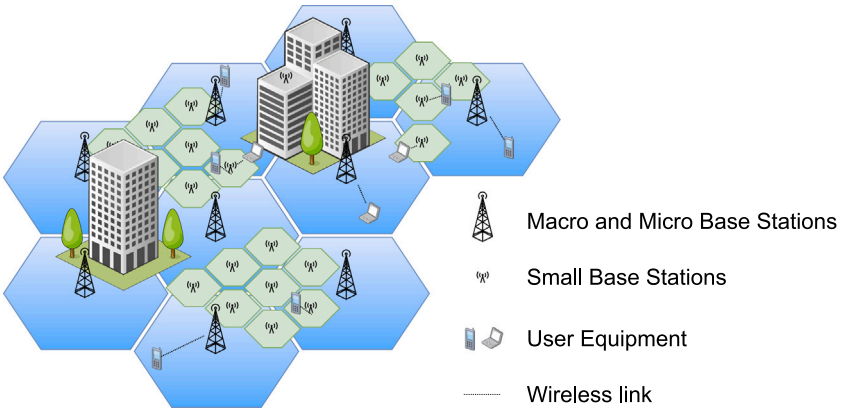

Fig. 1. An example of a UDN.

Several studies, such as [13], predict the density of 5G base stations (Small Base Stations, SBSs) to come up to 40–50 sites/km^2, but theoretical works exist in which SBS deployments with one-meter separation are characterized [6]. The main idea behind the network ultra-densification is to get the access nodes as close as possible to the end users. However, UDNs also lead to increased power consumption because of the large number of deployed SBSs (see Fig. 1). In fact, since the SBSs are responsible for 50 to 80 percent of the whole energy demand [14], densification will lead to unaffordable operational expenditures. In this context, an standardized approach by the 3rd Generation Partnership Project association [15] to save energy is the selective turning off of SBSs in periods in which the network is serving a low number of users. This problem, called the Cell Switch Off (CSO) problem [16], is NP-complete [17] and cannot only account for a reduction in energy consumption (a trivial solution might be to shut down the entire infrastructure), but also for any performance criterion that measures the Quality of Service (QoS) provided by the network. To this end, the network capacity has been considered in terms of the total bandwidth that can be served to users. Given the level of densification anticipated for real-world 5G networks, that is, the size of problem instances (the number of SBSs that could be switched on/off), a metaheuristic approach is used. Specifically, we elaborate on multi-objective metaheuristics that seek trade-off solutions between power consumption and network capacity [18,19].

This work is in the line of developing problem-specific search operators to improve the exploration of multi-objective metaheuristics, and significantly extends previous works [20,21]. Firstly, the problem modeling has been enhanced to incorporate additional real-world features of 5G networks, including a mmWave massive multiuser MIMO scenario in which several User Equipments (UEs) are communicating at the same time using connections towards high-frequency SBSs. Each of these SBSs now has several sectors, and each sector now installs multiple antennas grouped into radio frequency chains that define the cells (i.e., the area covered by the sector). Under this new modeling, two new search operators are proposed that take advantage of the network densification and sectorization of SBSs to reduce power consumption. The adaptation and extension of previously defined operators to the CSO problem in [20,21] have also been achieved. The effectiveness of all these operators has been evaluated by providing solid experimental evidence in nine different scenarios with different densification levels in the deployment of both SBS and UE. For each of these scenarios, 50 different instances have been randomly generated, thus considering 450 problem instances. We have engineered hybrid versions of multi-objective metaheuristics that encompass Pareto-based, indicator-based, and decomposition-based approaches to show that the problem-specific information introduced by the newly devised operators improves the search of the three main algorithmic groups within the domain. In particular, the solvers used are as follows: NSGA-II [22] and MOCell [23] (Pareto-based), as they have been used in our previous works [19–21], SMS-EMOA [24] (indicator-based), and MOEA/D [25]. Furthermore, since the solutions are represented by binary strings, where each bit corresponds to the state (on/off) of a cell, and we seek to reduce the power consumption over periods of low traffic demands (i.e., a small number of UEs), solutions may contain many bits set to zero. For this reason, we have also included in the comparison a recent and specialized algorithm called SparseEA [26], which targets precisely this kind of sparse optimization problems [27]. Using the Hypervolume (HV) [28], a Pareto-compliant quality indicator, the results have shown that newly devised operators have always improved the search of all the multi-objective metaheuristics considered, thus clearly enhancing their search capabilities for addressing the CSO problem.

The rest of the document is organized as follows: the next section elaborates on the work related to the CSO problem and how it has been addressed in the literature. Section 3 details the UDN system model and formulates the CSO problem objectives. The MOEAs used and the problem-specific operators designed for hybridization are described in Section 4. Section 5 develops the methodology used in the experimentation and analyzes the results obtained. The final section is devoted to summarizing the main conclusions of the work as well as the lines of future work.

2. Related work

The energy consumption of Information and Communication Technologies infrastructures (ICT) in general [29], and cellular networks in particular [30,31], has been an active research topic, specially in the last 20 years, in order to address the ever-increasing carbon footprint on the environment of this industry. The enabling technologies of 5G networks make the energy issue even worse, as has been clearly stated in recent surveys that have revised the different approaches proposed in the literature to reduce power consumption from different perspectives, ranging from advanced energy management strategies [32–37] to data-driven schemes based on Artificial Intelligence/Machine Learning [38,39]. Sustainability in UDNs has also attracted a lot of attention, as the massive deployment of SBSs is a key factor in power consumption, with surveys specifically aimed at this 5G paradigm [40–42].

Cell activation/deactivation is a common and useful technique for reducing energy consumption in all previously comprehensive reviews of the literature. Determining which SBSs are switched on or off requires the network first to serve a traffic demand, and the decision can be made either in an online (dynamic) [43] or offline (static) manner [44]. This work focuses on the latter approach, as radio network engineers are usually reluctant to undertake frequent SBS switching (e.g., at locations with large traffic fluctuations) and require their approval. The underlying problem, named the Cell Switch-Off (CSO) problem [16], is known to be NP-complete [17], and it has been tackled

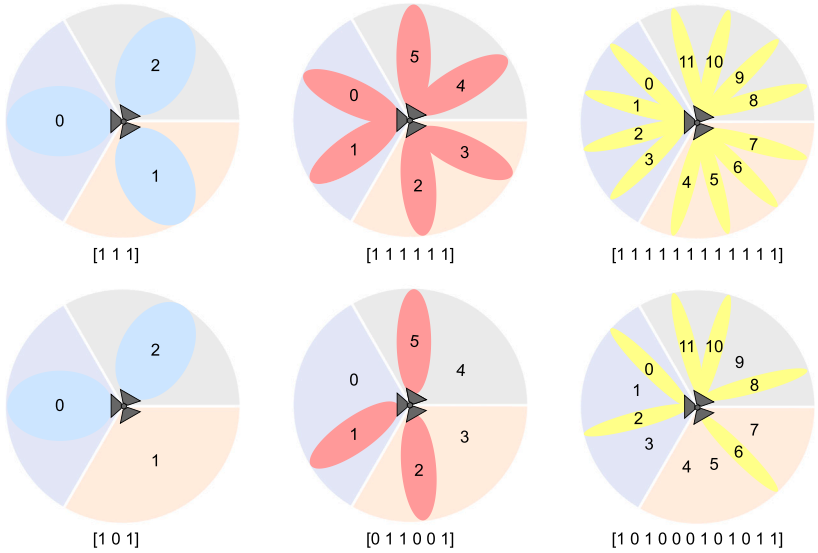

Fig. 2. Configuration of the SBSs, sectors and cells used in this work, as well as its mapping into a binary encoded representation.

Table 1
Model parameters for users and base stations.

Cell	Parameter	Eq.	LL	LM	LH	ML	MM	MH	HL	HM	HH
Micro	G_{tx}	(2)	12								
	f	(5)	5 GHz (BW = 500 MHz)								
	α	(8)	15								
	β	(8)	10000								
	δ	(8)	1								
	ρ [W]	(8)	1								
	n_{tx}		8								
	n_{rx}		2								
	λ_P^{micro} [Cells/km^2]		300	300	300	600	600	600	900	900	900
Pico	G_{tx}	(2)	20								
	f	(5)	20 GHz (BW = 2000 MHz)								
	α	(8)	9								
	β	(8)	6800								
	δ	(8)	0.5								
	ρ [W]	(8)	1								
	n_{tx}		64								
	n_{rx}		4								
	λ_P^{pico} [Cells/km^2]		1500	1500	1500	1800	1800	1800	2100	2100	2100
Femto	G_{tx}	(2)	28								
	f	(5)	68 GHz (BW = 6800 MHz)								
	α	(8)	5.5								
	β	(8)	4800								
	δ	(8)	0.2								
	ρ [W]	(8)	1								
	n_{tx}		256								
	n_{rx}		8								
	λ_P^{femto} [Cells/km^2]		3000	3000	3000	6000	6000	6000	9000	9000	9000
UEs	λ_P^{UE} [UE/km^2]		1000	2000	3000	1000	2000	3000	1000	2000	3000

with different approaches in the domain, such as clustering [45–47] or game theory [48]. This decision problem has also been defined as an optimization problem [17] and, within this research field, it has been addressed with exact [49,50], heuristic [51–53] and metaheuristic techniques [18,54]. Our work relies on this last set of methods, which embrace both single [55,56] and multi-objective approaches [19,57]. However, in the context of the CSO problem, apart from previous works from the authors [20,21], only canonical versions of metaheuristics have been used. It is well known that hybridization is a powerful tool for improving the search of these algorithms [58] but, to the best of our knowledge, this topic is still unexplored in the CSO literature. Under the new and more accurate modeling of the CSO problem, this work improves upon our previously published material by devising additional local search operators aimed at reducing the power consumption and also showing their suitability over MOEAs covering the most important trends in the domain, e.g., Pareto-based, decomposition-based, and indicator-based algorithms that, to the best of our knowledge, have never been hybridized (SMS-EMOA and MOEA/D, particularly) or even used before in the context of this problem (SparseEA). We have also evaluated the synergy between different operators, which also opens new promising lines of research.

3. The CSO problem

This section first introduces the modeling of the UDN and its parameters, and then describes the mathematical formulation of the CSO problem addressed.

3.1. UDN modeling

This work considers a service area of 500 × 500 meters, where ten different regions have been defined with different propagation conditions. To compute the received power at a given location of this area, P_{rx} [dBm], the following model has been used:

$$P_{rx}\ [\text{dBm}] = P_{tx}\ [\text{dBm}] + PLoss\ [\text{dB}] \tag{1}$$

where, P_{rx} is the received power in dBm, P_{tx} is the transmitted power in dBm, and $PLoss$ are the global signal losses, which depend on the given propagation region, and are computed as:

$$PLoss\ [\text{dB}] = GA + PA \tag{2}$$

where GA is the total gain of both antennas, and PA are the transmission losses in space, computed as:

$$PA\ [\text{dB}] = \left(\frac{\lambda}{4 \cdot \pi \cdot d}\right)^{K} \tag{3}$$

where d is the Euclidean distance to the corresponding sector at the SBS, K is the exponent loss, which randomly ranges in $[2.0, 4.0]$ for each of the 10 different regions. The Signal-to-Interference plus Noise Ratio (SINR) for UE k, is computed as:

$$SINR_k = \frac{P_{rx,j,k}\ [\text{mW}]}{\sum_{i=1}^{M} P_{rx,i,k}\ [\text{mW}] - P_{rx,j,k}\ [\text{mW}] + P_n\ [\text{mW}]} \tag{4}$$

where $P_{rx,j,k}$ is the received power by UE k from the cell j, the summation is the total received power by UE k from all the cells operating at the same frequency that j, and P_n is the noise power, computed as:

$$P_n\ [\text{dBm}] = -174 + 10 \cdot \log_{10} BW_j \tag{5}$$

being BW_j the bandwidth of cell j, defined as 10% of the SBS operating frequency, which is the same for all cells it deploys (see Table 1).

Finally, the UEs capacity has been calculated according to the MIMO depicted in [59]. Thus, we assume that the transmission power from each antenna is $P_{tx}/n_t x$, where $n_t x$ indicates the number of transmitting antennas. Then, if we consider the subchannels to be uncoupled, their capacities can add up, and the overall channel capacity of the UE k can be estimated using the Shannon capacity formula:

$$C_k^j[bps] = BW_k^j\ [\text{Hz}] \cdot \sum_{i=1}^{r} \log_2\left(1 + \frac{SINR_k \cdot \lambda_i}{n_{tx}}\right) \tag{6}$$

where $\sqrt{\lambda_i}$ is the singular value of the channel matrix $\mathbf{H}$, of dimensions $n_{rx} \times n_{tx}$ (i.e., # receiving antennas × # transmitting antennas). Note that both n_{rx} and n_{tx} depend on the cell type (see Table 1). BW_k^j is the bandwidth assigned to UE k when connected to the cell j, assuming round-robin scheduling, that is:

$$BW_k^j = \frac{BW_j}{N_j} \tag{7}$$

where N_j is the number of UEs connected to a cell j, and the UEs are connected to the cell that provides the highest SINR, regardless of its type.

In order to build a heterogeneous network, three different types of cells of increasing size and decreasing frequency are considered: femtocells, picocells and microcells. Recall that these cells are generated by the antennas installed in a given sector of an SBS. Fig. 2 illustrates the three configurations used in our modeling. In the first row, the three SBSs have the three sectors and all their cells switched on (in operation), thus the mapping to the binary string that represents a tentative solution, included below each subfigure, does have all the genes set to 1. In the second row, we have included several solutions with a subset of cells switched off, with the corresponding genes set to 0. It should also be noted that the number of transmitting antennas of each cell type increases with frequency, being 8, 64 and 256 transmitting antennas, respectively, for micro, pico, and femtocells. In the same way, we assume that high-capacity UEs, which will preferably connect to small cells (pico and femtocells), will implement a higher number of receiving antennas (4 and 8 for pico and femtocells, respectively).

With the system configuration described above, the actual deployment of the cells is carried out via the placement of SBSs in the working area, using a random rotation angle for the sectors, which determines the orientation of the different cell beams. Then, both SBSs and UEs are deployed using independent Poisson Point Processes (PPP) with different densities, defined by λ_P^{Cells} and λ_P^{UE}, respectively. We have implemented in our software framework a discretization approach that uses a grid of 100 × 100 points (also called "pixels" or area elements), each covering a 25 m^2 area, where the signal power is assumed to be constant. In addition to that, vertical densification has been taken into account by considering 3 vertical area elements, i.e., 25 meters of height. The purpose of this mechanism is to reduce the computational cost of calculating the SINR values.

The power consumption of a transmitter is computed based on the model presented in [3], which considers that the device is transmitting over the fiber backhauling. Therefore, the regular power consumption of cell j, P_j, is expressed as:

$$P_j = \alpha \cdot P + \beta + \delta \cdot S + \rho \tag{8}$$

where P denotes the transmitted or radiated power of the transmitter, the coefficient α represents the efficiency of the transmission power produced by a radio frequency amplifier and feeder losses, the power dissipated due to signal processing and site cooling is denoted by β and the dynamic power consumption per unit of data is given by δ, being S the actual traffic demand provided by the serving cell. Finally, the power consumption of the transmitting device is represented by the coefficient ρ. However, in order to consider an accurate power consumption model, the power consumed by the air conditioning and power supply of the SBS should be also taken into account [60]. This has been called maintenance power and is set to 2W/SBS for any SBS containing at least one active cell.

The detailed parametrization of the scenarios addressed is included in Table 1, in which column Eq. links the parameter to the corresponding equation in the formulation detailed above. The names in the last nine columns, XY, represent the deployment densities of SBSs and UEs, respectively, so that X = {L, M, H}, meaning either low, medium, or high-density deployments (λ_P^{Cell} parameter of the PPP), and Y = {L, M, H}, indicates a low, medium or high density of deployed UEs (λ_P^{UE} parameter of the PPP), in the last row of the table. The parameters G_{tx} and f of each type of cell refer to the transmission gain and the operating frequency (and its available bandwidth) of the antenna, respectively, being n_{tx} and n_{rx} the number of transmit and receive antennas. Finally, the parameters of the previously described power consumption model are also included. Nine instances have been therefore used in this work in order to assess the performance of the different metaheuristics and their hybridization with the problem-specific operators.

3.2. Problem formulation and objectives

Let $\mathcal{B}$ be the set of randomly deployed SBSs and C_b the set of cells installed in SBS b, with $b \in \mathcal{B}$. A solution to the CSO problem is a binary string s, where s_c^b indicates whether the cell c of a given SBS b is activated or not. The first objective to be minimized is, therefore, computed as:

$$\min f_{Power}(s) = \sum_{b}^{\mathcal{B}} P_b \sum_{c}^{C_b} s_c^b \tag{9}$$

where P_b is the power consumption of SBS b (Eq. (8)). Note that P_b includes both the transmission power of every cell $c \in P_b$ and its maintenance power.

Let $\mathcal{U}$ be the set of UEs also deployed as described in the previous section, and $\mathcal{U}$ the entire set of cells contained in $\mathcal{B}$. Subsequently, in order to compute the total capacity of the system, UEs are first

assigned to the active Cell that provides it with the highest SINR. Let $\mathcal{A}(s) \in \{0,1\}^{|\mathcal{U}|\times|\mathcal{C}|}$ be the matrix where $a_{ij} = 1$ if $s_j = 1$ and the Cell j serves UE i with the highest SINR, and $a_{ij} = 0$ otherwise. Then, the second objective to be maximized, which is the total capacity provided to all UEs, is calculated as:

$$\max f_{Cap}(s) = \sum_{i=1}^{|\mathcal{U}|}\sum_{j=1}^{|\mathcal{C}|} s_j \cdot a_{ij} \cdot C_i^j \tag{10}$$

where C_i^j is the capacity of Cell j provided to UE i (Eq. (7)). We would like to remark that these two problem objectives are clearly conflicting one each other, since switching off base stations leads to a reduction of the power consumption of the network, but it also damages the capacity received by the user, as the UE-Cell distance increases (rising the propagation losses) at the same time as the available bandwidth to serve users is reduced.

4. Hybridization: MOEAs used and newly developed operators for the CSO problem

This section first describes briefly the MOEAs used in this work. Then, the problem-specific operators devised for the CSO problem are detailed. The last part is devoted to showing how these operators are integrated within the evolutionary loop of the chosen multi-objective metaheuristics.

4.1. Multi-objective evolutionary algorithms

In the last decades, Evolutionary Algorithms (EAs) have shown their effectiveness in solving different optimization and search problems. In addition, one of the most interesting capabilities of these algorithms is the ability to deal with multi-objective optimization problems. Since its proposal in the 1990s, Multi-Objective Evolutionary Algorithms (MOEAs) have been widely used for the resolution of several complex problems with two or three conflicting objectives in various branches of engineering, science, and commerce. If the problems have more conflicting objectives, the research community has proposed different alternatives, since MOEAs lose performance when the number of conflicting objectives increases [61,62].

In order to address the optimization problem stated in this paper, the following five MOEAs have been chosen from the specialized literature: NSGA-II (*Non-dominated Sorting Genetic Algorithm II*) [22], MOCell (*Multi-Objective Cellular Genetic Algorithm*) [23], SMS-EMOA (*S Metric Selection Evolutionary Multi-Objective Algorithm*) [24], MOEA/D (*Multi-Objective Evolutionary Algorithm based on Decomposition*) [25] and SparseEA [26].

The first four algorithms are well known in the literature and have been selected to cover the three main paradigms for solving multi-objective optimization problems (MOPs), namely, Pareto-based, indicator-based, and decomposition-based. NSGA-II and MOCell are representative of Pareto-based approaches that have already been used in previous works by the authors in the context of the CSO problem. They use ranking to identify non-dominated solutions, and crowding as a density estimator to promote these non-dominated solutions of the less populated areas of the approximated Pareto fronts. This latter operator is rather computationally expensive, but improved implementations exist [63]. As an indicator-based algorithm, we have chosen SMS-EMOA, whose search engine is guided by Hypervolume. And finally, MOEA/D covers the decomposition-based paradigm. SparseEA deserves special attention, as it is a recent algorithmic proposal specifically aimed at solving sparse MOPs, i.e., large-scale binary-encoded MOPs in which most of the decision variables are zero [64]. This is potentially the context of the CSO problem, as it tries to switch off as many cells as possible in periods of low traffic demands to reduce power consumption. To do so, SparseEA uses a similar scheme as NSGA-II in terms of crossover, selection, ranking and crowding, but it applies tailored strategies to generate the initial population and the offspring that aim at ensuring the sparsity of the solutions generated. This algorithm uses a hybrid representation of the solutions (real and binary vectors), where the real vector stores the best values of the decision variables found so far, and the binary vector stores the decision variables that should be set to zero to control the sparsity of solutions.

4.2. Hybridization with problem-specific operators

The integration of problem-specific operators in the evolutionary cycle is done after the application of the genetic operators, as shown in Algorithm 1. Each specific operator is applied with a probability $rate_{operator}$ defined in $[0,1]$. For multi-operator hybrids, the following order is used: $EC^{\downarrow}$, $SC^{\downarrow}$, $PF^{\uparrow}$, $PSC^{\uparrow}$ and $HF^{\uparrow}$. Hence, all, some, or none could be potentially applied.

4.3. Problem-specific operators

We have defined five different local search operators that are aimed at exploiting problem-specific information that can guide the search of MOEAs towards regions of higher quality solutions. These operators mainly target switching cells either on or off, so their acronyms have used a superscript with a ↑ or ↓, respectively, to better show this fact and enhance the reading. They all have linear computational complexity, thus not substantially increasing the runtime.

4.3.1. $EC^{\downarrow}$: Empty cell operator

As a consequence of SBS densification and sectorization, many cells may result to be empty, i.e., not providing service to any user, so that it can be switched off. In order to incorporate this useful information about the network into the algorithm search, the *Empty Cell* operator, or $EC^{\downarrow}$ for short, has been designed. It explores all cells of the candidate solution, switching off those that are not serving any UE, as it is illustrated in Algorithm 2. Despite its apparent simplicity, this operator promotes a considerable intensification capacity. It is remarkable that, when applied without any restriction, the $EC^{\downarrow}$ operator can disrupt the evolution of the algorithm, since it prevents the generation of solutions that reassign users to such empty cells, since they would all be switched off after the action of the operator. In order to address this issue, the operator is applied with a certain rate.

4.3.2. $SC^{\downarrow}$: Single cell operator

Having multiple sectors/cells within a single SBS introduces new optimization possibilities to improve the search capabilities of the algorithms. In particular, the Single Cell operator ($SC^{\downarrow}$) aims to explore low power consumption solutions by switching off base stations that have only one single active cell, saving in this way the power consumed by the air conditioning and power supply of the entire SBS. Again, when applied without restrictions, this operator might lead to solutions in which some important base stations might be switched off, regardless of the number of users that were assigned to them. This fact could significantly disrupt the search of the MOEAs. For that reason, this operator is applied with a given rate. Algorithm 3 sketches the pseudocode of the operator.

4.3.3. $PF^{\uparrow}$ And $PSC^{\uparrow}$: Prioritize femto and prioritize small cells operators

In contrast to the previous specific operators, which aim to intensify the search in areas of low energy consumption, the *Prioritize Femto Cells* and *Prioritize Small Cells* operators aim to intensify it in the area of the highest capacity. These operators seek active cells that offer an SINR level higher than a threshold over the SINR of users with the cells to which they are assigned. After experiments with values from 1 dB to 9 dB, the threshold value was set at 1 dB, as it was the one with the best results. In addition, this value allows us to maintain consistency with previous works [21]. The difference between the two operators lies in the set of candidate UEs to participate in the search:

Algorithm 1: Pseudocode of the hybridization with problem-specific operators.

```
t ← 0                                                    // Generation counter
A(t) ← ∅                                                 // Archive for non-dominated solutions
S(t) ← GenerateInitialPopulation()                       // Current population
Evaluate(S(t))                                           // Evaluate the problem objectives
A(t) ← Update(A(t), S(t))                                // Obtain the non-dominated solutions from S(0)
while not StoppingCondition() do
   t ← t + 1
   S(t) ← Selection(S(t − 1), A(t − 1))                  // Select solutions for mating
   S(t) ← Variation(S(t), A(t − 1))                      // Apply variation operators (crossover, mutation)
                                                         // using the mating population and the archive
   for all s ∈ S(t) do
      r1 ← Random(0, 1)                                  // Draw a random number in [0,1]
      if r1 < rate_Operator1 then
         s ← Operator1(s)                                // Apply Operator1 to solution s
      end if
      r2 ← Random(0, 1)
      if r2 < rate_Operator2 then
         s ← Operator2(s)                                // Apply Operator2 to solution s
      end if
      ...
      rn ← Random(0, 1)
      if rn < rate_OperatorN then
         s ← OperatorN(s)                                // Apply OperatorN to solution s
      end if
   end for
   Evaluate(S(t))
   A(t) ← Update(A(t − 1), S(t))                         // Obtain the non-dominated solutions from the
                                                         // current population S(t) and the archive A(t-1)
   S(t) ← Replacement(S(t), A(t))                        // Replace solutions in the current population
end while
Output: A(t)
```

Algorithm 2: Pseudocode of the $EC^{\downarrow}$ operator.

```
C ← cells(UDN)
for c ∈ C do
   if ConnectedUEs(c) == 0 then
      SwitchOff(c)
   end if
end for
```

Algorithm 3: Pseudocode of the $SC^{\downarrow}$ operator.

```
B ← SBSs(UDN)
for b ∈ B do
   if ActiveCells(b) == 1 then
      c ← ActiveCell(b)
      SwitchOff(c)
   end if
end for
```

Prioritize Femto Cells only concerns the UDN UEs that are not assigned to femtocells; *Prioritize Small Cells* is less restrictive, using the UEs that are not assigned to small cells, that is, microcells and macrocells. After switching on the cell that meets the SINR threshold, if any, the operator switches off all cells that have no UEs assigned to them. Therefore, the $EC^{\downarrow}$ is likely to be applied as a final step. Algorithm 4 shows the pseudocode of the two operators, which differs only in the initial set of cells.

4.3.4. $HF^{\uparrow}$: Higher frequency operator

Similar to $PF^{\uparrow}$ and $PSC^{\uparrow}$ operators, the purpose of the *Higher Frequency* operator is to intensify the search towards the capacity objective. This operator seeks to take advantage of the capacity improvements that can be offered by smaller cells with a higher operating frequency than those serving UEs. Thus, this operator turns on cells of the same SBSs to which the UEs are assigned and that offer a higher SINR than the one they already have. Furthermore, if the cell to which the UEs are assigned only serves one, the cell is turned off to encourage the UEs to be assigned to the activated cell, thus promoting the increase of capacity as well as the reduction of the power consumption, as illustrated in Algorithm 5.

Algorithm 4: Pseudocode of the $PF^{\uparrow}$ and $PSC^{\uparrow}$ operators.

```
if PF↑ then
   U ← UsersNotServedByFemtoCells(UDN)
else if PSC↑ then
   U ← UsersNotServedBySmallCells(UDN)
end if

for u ∈ U do
   current ← GetServingCell(u)
   C ← GetFemtoCellsWithHigherSINR(u)
   for c ∈ C do
      if SINR(u, c) > 1 dB then
         SwitchOn(c)
         if GetAssignedUsers(current) == 1 then
            SwitchOff(current)
         end if
         break
      end if
   end for
end for
SwitchOffEmptyCells()
```

5. Experimentation

This section describes the methodology used to conduct the experiments, showing the effectiveness of the new hybrid proposals, as well as the analysis of the results obtained.

5.1. Methodology

Based on the nine scenarios described in Section 3 and the stochastic nature of the metaheuristics, 50 seeds have been addressed in the experimentation for each type of scenario. This ensures that all algorithms face the same set of problem instances.

Algorithm 5: Pseudocode of the $HF^{\uparrow}$ operator.

```
U ← GetUsers(UDN)
for u ∈ U do
    b ← GetServingBTS(u)
    best ← GetServingCell(u)
    current ← best
    for c ∈ GetCellsWithHigherOperatingFrequency(b) do
        if SINR(u,c) ≥ SINR(u,best) then
            best ← c
        end if
    end for
end for
SwitchOn(best)
if GetAssignedUsers(current) == 1 then
    SwitchOff(current)
end if
```

In order to obtain fair comparative results between algorithms, they all use the same population size of 100 solutions and the same genetic operators: binary tournament selection, two-point crossover with a crossover rate of 0.9, and bit-flip mutation with a mutation rate of $1/L$, being L the number of cells in the scenario. SparseEA is the exception because its own framework is designed to maintain sparsity in solutions, and changing its genetic operators to general-purpose ones would cause the algorithm to lose its distinguishing features from the others. Moreover, MOEA/D has also used a binary tournament to select two parents for crossover.

The stopping condition is defined as a maximum number of function evaluations, which increases with the density of deployed SBSs, that is, with the size of the instance. The following values have been set up: 100,000 evaluations for L{X}; 150,000 evaluations for M{X}; and 250,000 evaluations for H{X}, (being {X} the three densities of the UEs). These values are obtained after a preliminary study that has shown that they are enough to guarantee the convergence of the algorithms.

With respect to the specific operators, the first step has been to conduct experiments with them separately to clearly isolate their impact on the search of the different MOEAs. For this purpose, we have initially defined the following application rates: 0.1, 0.05, 0.01, 0.005 and 0.001. However, after briefly analyzing the results, the two smaller ones, 0.05 and 0.005, have not been considered anymore in this work, as they have provided negligible contributions to the quality of the solutions reached. We have also removed these two settings to increase the readability of the results. Bearing all this in mind, this part of the experiments accounted for a total of 67,500 runs. A final set of experiments carried out to analyze potential synergies between the problem-specific operators in the hybrid MOEAs has involved 5 MOEAs, 5 operators, 5 application rates, 14 combinations between operators, 9 scenarios, and 50 seeds, which amounts to 31,500 additional runs. All of them have required roughly about 18.4 years of CPU time. In order to afford such computational demands, the experiments have been deployed in the facilities of the Supercomputing and Bioinformatics Center of the Universidad de Málaga, named Picasso. It is a heterogeneous computing platform composed of several clusters with up to 30.616 computing cores. The full hardware description can be found in http://www.scbi.uma.es/site/scbi/hardware.

Two indicators have been used to measure the quality of the approximations to the Pareto front achieved by the different algorithms: the attainment surfaces [65] and Hypervolume (HV) [28]. The empirical attainment function (EAF) [65] allows undertaking a graphical analysis of the approximated fronts. Indeed, EAF graphically displays the expected performance and its variability of the approximated Pareto fronts obtained by the multi-objective algorithm over multiple runs. Informally, the 50%-attainment surface in the multi-objective domain, which is chosen here, is analogous to the median value in the single-objective one. The HV, in turn, is a Pareto-compliant, single-value-based quality indicator considered in the multi-objective community as one of the most reliable measures to compare approximations to the Pareto front of different algorithms. Its values depend, however, on the arbitrary scale of the objective function values, so a normalization procedure is required to avoid misleading results. To do so, and since the problem addressed in this paper is a realistic NP-complete combinatorial optimization problem for which we do not have the true Pareto front, a reference Pareto front (RPF) has been built for each instance of the problem. This RPF is composed of all the non-dominated solutions found by all the algorithms involved in these experiments, and is used to normalize the approximated fronts reached by the algorithms prior to calculating the HV value. Non-dominated solutions outside of the limits of the corresponding RFP are discarded (i.e., their contribution to the HV is zero).

Table 2
Median and IQR of HV for the canonical MOEAs.

	NSGA-II	MOCell	SMS-EMOA	MOEA/D	SparseEA
LL	$0.521_{0.170}$	$0.296_{0.188}$	$0.642_{0.150}$	$0.000_{0.000}$	$0.212_{0.051}$
LM	$0.520_{0.185}$	$0.266_{0.193}$	$0.594_{0.125}$	$0.000_{0.000}$	$0.208_{0.069}$
LH	$0.449_{0.161}$	$0.258_{0.198}$	$0.556_{0.133}$	$0.000_{0.000}$	$0.216_{0.055}$
ML	$0.271_{0.170}$	$0.434_{0.212}$	$0.519_{0.137}$	$0.000_{0.000}$	$0.165_{0.045}$
MM	$0.193_{0.231}$	$0.303_{0.183}$	$0.437_{0.141}$	$0.000_{0.000}$	$0.173_{0.041}$
MH	$0.210_{0.285}$	$0.036_{0.194}$	$0.435_{0.191}$	$0.000_{0.000}$	$0.181_{0.040}$
HL	$0.365_{0.249}$	$0.005_{0.199}$	$0.579_{0.161}$	$0.000_{0.000}$	$0.153_{0.036}$
HM	$0.179_{0.265}$	$0.000_{0.035}$	$0.438_{0.160}$	$0.000_{0.000}$	$0.145_{0.042}$
HH	$0.177_{0.265}$	$0.000_{0.075}$	$0.407_{0.204}$	$0.000_{0.000}$	$0.155_{0.040}$

In order to provide these HV results with statistical significance [66], a Kolmogorov–Smirnov test is first performed to check whether the 50 samples are distributed according to a normal distribution or not. If so, an ANOVA I test is performed; otherwise, a Kruskal–Wallis test is performed. Since more than two algorithms are involved in the study, a post hoc testing phase that allows for multiple comparisons of samples (multicompare) has been conducted. All statistical tests are performed with a confidence level of 95%. The stats output is shown in a tabular form, as a head-to-head comparison between pairs of algorithms; a black upward triangle says that the setting of the row has statistically higher values than the configuration of the column, and a white downward triangle states that the configuration in the row has statistically lower values than the configuration in the column. When no statistically significant differences are found, the spot is left empty. We have also computed the Friedman rank sum test with Holm correction to support several rankings among the algorithms that are undertaken in the result analyses below.

Both the generated data and the statistical tests can be found as supplementary material at https://doi.org/10.6084/m9.figshare.21378000. All the software and the scenarios used can be also downloaded from https://github.com/galeanobra/CSO_Hybrid in order to guarantee the reproducibility of the experimentation. In the following sections, we have structured all this information in a readable form to ease the analysis of the results and to better support our conclusions.

5.2. Results

This section has been structured into two separated parts: the first one aims at showing how the problem-specific operators devised in this work (and described in Section 4.3) improve the search of the five MOEAs in which they have been incorporated; as these operators have different intensification capabilities towards a given objective (either the energy consumption or the network capacity), the second part is devoted to analyzing potential synergies between them, when applying several of such operators simultaneously.

Table 3
Median and IQR of the HV indicator for NSGA-II in the nine scenarios.

	Canonical	$EC^{\downarrow}$			$SC^{\downarrow}$			$PF^{\uparrow}$			$PSC^{\uparrow}$			$HF^{\uparrow}$		
		0.1	**0.01**	**0.001**	**0.1**	**0.01**	**0.001**	**0.1**	**0.01**	**0.001**	**0.1**	**0.01**	**0.001**	**0.1**	**0.01**	**0.001**
LL	$0.521_{0.170}$	$0.766_{0.076}$	$0.748_{0.104}$	$0.668_{0.219}$	$0.539_{0.187}$	$0.608_{0.119}$	$0.541_{0.158}$	$0.744_{0.079}$	$0.758_{0.080}$	$0.589_{0.211}$	$0.732_{0.082}$	$0.735_{0.100}$	$0.571_{0.232}$	$0.528_{0.226}$	$0.536_{0.200}$	$0.505_{0.162}$
LM	$0.520_{0.185}$	$0.747_{0.071}$	$0.720_{0.081}$	$0.621_{0.247}$	$0.510_{0.149}$	$0.555_{0.131}$	$0.519_{0.130}$	$0.700_{0.087}$	$0.693_{0.092}$	$0.533_{0.185}$	$0.687_{0.121}$	$0.671_{0.148}$	$0.530_{0.184}$	$0.486_{0.167}$	$0.467_{0.160}$	$0.514_{0.134}$
LH	$0.449_{0.161}$	$0.719_{0.086}$	$0.671_{0.068}$	$0.546_{0.228}$	$0.441_{0.154}$	$0.504_{0.147}$	$0.438_{0.162}$	$0.648_{0.122}$	$0.639_{0.126}$	$0.479_{0.227}$	$0.648_{0.097}$	$0.644_{0.082}$	$0.500_{0.175}$	$0.413_{0.164}$	$0.449_{0.184}$	$0.452_{0.165}$
ML	$0.271_{0.170}$	$0.739_{0.076}$	$0.713_{0.102}$	$0.658_{0.167}$	$0.261_{0.191}$	$0.412_{0.193}$	$0.327_{0.222}$	$0.717_{0.095}$	$0.717_{0.105}$	$0.624_{0.366}$	$0.710_{0.109}$	$0.710_{0.106}$	$0.572_{0.466}$	$0.280_{0.199}$	$0.262_{0.141}$	$0.282_{0.203}$
MM	$0.193_{0.231}$	$0.707_{0.070}$	$0.689_{0.096}$	$0.617_{0.243}$	$0.150_{0.248}$	$0.286_{0.204}$	$0.228_{0.241}$	$0.668_{0.103}$	$0.667_{0.100}$	$0.362_{0.493}$	$0.665_{0.092}$	$0.640_{0.126}$	$0.367_{0.398}$	$0.183_{0.260}$	$0.179_{0.224}$	$0.207_{0.219}$
MH	$0.210_{0.285}$	$0.668_{0.092}$	$0.657_{0.129}$	$0.513_{0.313}$	$0.210_{0.279}$	$0.312_{0.215}$	$0.266_{0.263}$	$0.622_{0.163}$	$0.606_{0.147}$	$0.416_{0.501}$	$0.589_{0.155}$	$0.607_{0.147}$	$0.295_{0.356}$	$0.165_{0.325}$	$0.191_{0.298}$	$0.184_{0.246}$
HL	$0.365_{0.249}$	$0.714_{0.082}$	$0.714_{0.096}$	$0.683_{0.146}$	$0.306_{0.260}$	$0.480_{0.218}$	$0.366_{0.281}$	$0.712_{0.106}$	$0.720_{0.095}$	$0.697_{0.187}$	$0.695_{0.104}$	$0.709_{0.090}$	$0.671_{0.151}$	$0.320_{0.201}$	$0.339_{0.263}$	$0.334_{0.294}$
HM	$0.179_{0.265}$	$0.653_{0.093}$	$0.636_{0.119}$	$0.583_{0.162}$	$0.189_{0.226}$	$0.321_{0.232}$	$0.253_{0.188}$	$0.619_{0.129}$	$0.613_{0.133}$	$0.595_{0.237}$	$0.616_{0.100}$	$0.628_{0.108}$	$0.584_{0.172}$	$0.176_{0.180}$	$0.186_{0.250}$	$0.192_{0.197}$
HH	$0.177_{0.265}$	$0.633_{0.088}$	$0.600_{0.103}$	$0.539_{0.187}$	$0.191_{0.263}$	$0.276_{0.229}$	$0.165_{0.241}$	$0.603_{0.134}$	$0.592_{0.118}$	$0.400_{0.418}$	$0.600_{0.089}$	$0.598_{0.125}$	$0.517_{0.288}$	$0.160_{0.260}$	$0.126_{0.256}$	$0.158_{0.302}$

Table 4
Median and IQR of the HV indicator for MOCell in the nine scenarios.

	Canonical	$EC^{\downarrow}$			$SC^{\downarrow}$			$PF^{\uparrow}$			$PSC^{\uparrow}$			$HF^{\uparrow}$		
		0.1	**0.01**	**0.001**	**0.1**	**0.01**	**0.001**	**0.1**	**0.01**	**0.001**	**0.1**	**0.01**	**0.001**	**0.1**	**0.01**	**0.001**
LL	$0.296_{0.188}$	$0.720_{0.073}$	$0.672_{0.114}$	$0.450_{0.362}$	$0.276_{0.221}$	$0.387_{0.175}$	$0.318_{0.201}$	$0.626_{0.096}$	$0.612_{0.153}$	$0.394_{0.260}$	$0.615_{0.110}$	$0.620_{0.148}$	$0.428_{0.308}$	$0.279_{0.160}$	$0.291_{0.204}$	$0.313_{0.221}$
LM	$0.266_{0.193}$	$0.677_{0.094}$	$0.595_{0.117}$	$0.472_{0.226}$	$0.297_{0.185}$	$0.366_{0.164}$	$0.302_{0.222}$	$0.557_{0.134}$	$0.519_{0.149}$	$0.385_{0.267}$	$0.624_{0.152}$	$0.607_{0.119}$	$0.621_{0.092}$	$0.474_{0.173}$	$0.522_{0.141}$	$0.523_{0.137}$
LH	$0.258_{0.198}$	$0.623_{0.088}$	$0.567_{0.117}$	$0.349_{0.323}$	$0.256_{0.229}$	$0.352_{0.239}$	$0.300_{0.266}$	$0.497_{0.137}$	$0.448_{0.278}$	$0.292_{0.229}$	$0.563_{0.155}$	$0.585_{0.141}$	$0.568_{0.109}$	$0.397_{0.147}$	$0.464_{0.149}$	$0.476_{0.143}$
ML	$0.434_{0.212}$	$0.691_{0.101}$	$0.725_{0.100}$	$0.511_{0.430}$	$0.002_{0.122}$	$0.531_{0.167}$	$0.535_{0.159}$	$0.657_{0.127}$	$0.632_{0.157}$	$0.650_{0.116}$	$0.610_{0.134}$	$0.611_{0.131}$	$0.532_{0.407}$	$0.005_{0.090}$	$0.176_{0.432}$	$0.423_{0.201}$
MM	$0.303_{0.183}$	$0.718_{0.070}$	$0.680_{0.078}$	$0.644_{0.080}$	$0.305_{0.154}$	$0.418_{0.166}$	$0.407_{0.160}$	$0.589_{0.134}$	$0.571_{0.138}$	$0.570_{0.140}$	$0.552_{0.156}$	$0.547_{0.131}$	$0.568_{0.126}$	$0.244_{0.200}$	$0.292_{0.242}$	$0.305_{0.223}$
MH	$0.036_{0.194}$	$0.591_{0.132}$	$0.559_{0.157}$	$0.305_{0.438}$	$0.003_{0.169}$	$0.125_{0.245}$	$0.057_{0.203}$	$0.467_{0.184}$	$0.453_{0.197}$	$0.278_{0.405}$	$0.505_{0.163}$	$0.485_{0.223}$	$0.486_{0.201}$	$0.195_{0.257}$	$0.273_{0.165}$	$0.291_{0.229}$
HL	$0.005_{0.199}$	$0.679_{0.103}$	$0.656_{0.128}$	$0.593_{0.176}$	$0.000_{0.129}$	$0.160_{0.253}$	$0.046_{0.241}$	$0.608_{0.109}$	$0.610_{0.118}$	$0.567_{0.262}$	$0.620_{0.113}$	$0.617_{0.127}$	$0.552_{0.176}$	$0.317_{0.295}$	$0.362_{0.282}$	$0.422_{0.246}$
HM	$0.000_{0.035}$	$0.583_{0.094}$	$0.556_{0.128}$	$0.453_{0.206}$	$0.000_{0.065}$	$0.077_{0.173}$	$0.000_{0.068}$	$0.488_{0.156}$	$0.502_{0.139}$	$0.417_{0.254}$	$0.525_{0.148}$	$0.495_{0.124}$	$0.377_{0.536}$	$0.150_{0.245}$	$0.197_{0.251}$	$0.217_{0.228}$
HH	$0.000_{0.075}$	$0.559_{0.109}$	$0.507_{0.120}$	$0.410_{0.240}$	$0.000_{0.073}$	$0.045_{0.186}$	$0.000_{0.131}$	$0.431_{0.182}$	$0.437_{0.206}$	$0.197_{0.402}$	$0.453_{0.137}$	$0.437_{0.181}$	$0.381_{0.258}$	$0.061_{0.247}$	$0.146_{0.264}$	$0.084_{0.313}$

Table 5
Median and IQR of the HV indicator for SMS-EMOA in the nine scenarios.

	Canonical	$EC^{\downarrow}$			$SC^{\downarrow}$			$PF^{\uparrow}$			$PSC^{\uparrow}$			$HF^{\uparrow}$		
		0.1	**0.01**	**0.001**	**0.1**	**0.01**	**0.001**	**0.1**	**0.01**	**0.001**	**0.1**	**0.01**	**0.001**	**0.1**	**0.01**	**0.001**
LL	$0.642_{0.150}$	$0.734_{0.105}$	$0.720_{0.108}$	$0.719_{0.070}$	$0.641_{0.135}$	$0.691_{0.093}$	$0.683_{0.086}$	$0.716_{0.085}$	$0.706_{0.072}$	$0.714_{0.087}$	$0.714_{0.110}$	$0.692_{0.081}$	$0.703_{0.106}$	$0.620_{0.139}$	$0.621_{0.136}$	$0.658_{0.132}$
LM	$0.594_{0.125}$	$0.721_{0.074}$	$0.709_{0.080}$	$0.714_{0.090}$	$0.606_{0.132}$	$0.672_{0.104}$	$0.658_{0.107}$	$0.697_{0.078}$	$0.701_{0.086}$	$0.699_{0.117}$	$0.700_{0.084}$	$0.682_{0.109}$	$0.681_{0.120}$	$0.562_{0.141}$	$0.597_{0.131}$	$0.633_{0.154}$
LH	$0.556_{0.133}$	$0.685_{0.078}$	$0.679_{0.108}$	$0.676_{0.096}$	$0.547_{0.100}$	$0.640_{0.122}$	$0.633_{0.117}$	$0.638_{0.101}$	$0.646_{0.095}$	$0.644_{0.103}$	$0.646_{0.110}$	$0.647_{0.102}$	$0.629_{0.116}$	$0.532_{0.126}$	$0.542_{0.146}$	$0.566_{0.111}$
ML	$0.519_{0.137}$	$0.725_{0.132}$	$0.690_{0.105}$	$0.698_{0.066}$	$0.500_{0.180}$	$0.624_{0.073}$	$0.614_{0.120}$	$0.691_{0.098}$	$0.686_{0.104}$	$0.688_{0.160}$	$0.692_{0.093}$	$0.682_{0.095}$	$0.683_{0.112}$	$0.456_{0.208}$	$0.509_{0.173}$	$0.500_{0.151}$
MM	$0.437_{0.141}$	$0.694_{0.108}$	$0.694_{0.086}$	$0.659_{0.079}$	$0.446_{0.173}$	$0.582_{0.141}$	$0.565_{0.101}$	$0.650_{0.083}$	$0.668_{0.092}$	$0.650_{0.114}$	$0.668_{0.064}$	$0.661_{0.089}$	$0.646_{0.098}$	$0.366_{0.220}$	$0.431_{0.217}$	$0.440_{0.195}$
MH	$0.435_{0.191}$	$0.653_{0.101}$	$0.651_{0.124}$	$0.666_{0.095}$	$0.375_{0.229}$	$0.553_{0.144}$	$0.533_{0.150}$	$0.632_{0.112}$	$0.629_{0.160}$	$0.642_{0.130}$	$0.628_{0.144}$	$0.622_{0.116}$	$0.625_{0.141}$	$0.360_{0.238}$	$0.437_{0.219}$	$0.407_{0.231}$
HL	$0.579_{0.161}$	$0.707_{0.086}$	$0.689_{0.094}$	$0.697_{0.101}$	$0.565_{0.136}$	$0.643_{0.108}$	$0.652_{0.110}$	$0.681_{0.075}$	$0.678_{0.079}$	$0.679_{0.096}$	$0.683_{0.099}$	$0.674_{0.108}$	$0.679_{0.078}$	$0.549_{0.168}$	$0.584_{0.147}$	$0.574_{0.159}$
HM	$0.438_{0.160}$	$0.616_{0.108}$	$0.616_{0.104}$	$0.629_{0.101}$	$0.429_{0.172}$	$0.553_{0.134}$	$0.552_{0.117}$	$0.627_{0.087}$	$0.621_{0.126}$	$0.594_{0.095}$	$0.613_{0.107}$	$0.609_{0.085}$	$0.611_{0.109}$	$0.345_{0.168}$	$0.414_{0.195}$	$0.415_{0.166}$
HH	$0.407_{0.204}$	$0.615_{0.089}$	$0.604_{0.110}$	$0.612_{0.122}$	$0.402_{0.199}$	$0.540_{0.102}$	$0.523_{0.139}$	$0.594_{0.123}$	$0.585_{0.124}$	$0.591_{0.105}$	$0.575_{0.120}$	$0.594_{0.096}$	$0.569_{0.124}$	$0.354_{0.229}$	$0.385_{0.158}$	$0.394_{0.173}$

Table 6
Median and IQR of the HV indicator for MOEA/D in the nine scenarios.

	Canonical	$EC^{\downarrow}$			$SC^{\downarrow}$			$PF^{\uparrow}$			$PSC^{\uparrow}$			$HF^{\uparrow}$		
		0.1	**0.01**	**0.001**	**0.1**	**0.01**	**0.001**	**0.1**	**0.01**	**0.001**	**0.1**	**0.01**	**0.001**	**0.1**	**0.01**	**0.001**
LL	$0.000_{0.000}$	$0.002_{0.089}$	$0.000_{0.069}$	$0.000_{0.024}$	$0.000_{0.000}$	$0.000_{0.030}$	$0.000_{0.022}$	$0.000_{0.036}$	$0.000_{0.046}$	$0.000_{0.048}$	$0.011_{0.143}$	$0.000_{0.062}$	$0.000_{0.063}$	$0.000_{0.000}$	$0.000_{0.000}$	$0.000_{0.000}$
LM	$0.000_{0.000}$	$0.000_{0.032}$	$0.000_{0.025}$	$0.000_{0.000}$	$0.000_{0.000}$	$0.000_{0.012}$	$0.000_{0.000}$	$0.000_{0.000}$	$0.000_{0.000}$	$0.000_{0.000}$	$0.000_{0.004}$	$0.000_{0.000}$	$0.000_{0.000}$	$0.000_{0.000}$	$0.000_{0.000}$	$0.000_{0.000}$
LH	$0.000_{0.000}$	$0.000_{0.011}$	$0.000_{0.002}$	$0.000_{0.007}$	$0.000_{0.000}$	$0.000_{0.000}$	$0.000_{0.000}$	$0.000_{0.000}$	$0.000_{0.000}$	$0.000_{0.000}$	$0.000_{0.000}$	$0.000_{0.000}$	$0.000_{0.000}$	$0.000_{0.000}$	$0.000_{0.000}$	$0.000_{0.000}$
ML	$0.000_{0.000}$	$0.043_{0.125}$	$0.022_{0.132}$	$0.027_{0.097}$	$0.000_{0.000}$	$0.000_{0.000}$	$0.000_{0.000}$	$0.004_{0.074}$	$0.000_{0.047}$	$0.000_{0.045}$	$0.044_{0.131}$	$0.008_{0.106}$	$0.000_{0.104}$	$0.000_{0.000}$	$0.000_{0.000}$	$0.000_{0.000}$
MM	$0.000_{0.000}$	$0.000_{0.057}$	$0.000_{0.039}$	$0.000_{0.047}$	$0.000_{0.000}$	$0.000_{0.000}$	$0.000_{0.000}$	$0.000_{0.003}$	$0.000_{0.015}$	$0.000_{0.056}$	$0.000_{0.084}$	$0.000_{0.030}$	$0.000_{0.020}$	$0.000_{0.000}$	$0.000_{0.000}$	$0.000_{0.000}$
MH	$0.000_{0.000}$	$0.000_{0.042}$	$0.000_{0.059}$	$0.000_{0.029}$	$0.000_{0.000}$	$0.000_{0.018}$	$0.000_{0.000}$	$0.000_{0.015}$	$0.000_{0.001}$	$0.000_{0.000}$	$0.000_{0.043}$	$0.000_{0.000}$	$0.000_{0.027}$	$0.000_{0.000}$	$0.000_{0.000}$	$0.000_{0.000}$
HL	$0.000_{0.000}$	$0.035_{0.158}$	$0.043_{0.173}$	$0.000_{0.158}$	$0.000_{0.000}$	$0.000_{0.031}$	$0.000_{0.009}$	$0.020_{0.126}$	$0.003_{0.121}$	$0.006_{0.085}$	$0.030_{0.170}$	$0.046_{0.144}$	$0.024_{0.142}$	$0.000_{0.000}$	$0.000_{0.002}$	$0.000_{0.000}$
HM	$0.000_{0.000}$	$0.036_{0.114}$	$0.020_{0.103}$	$0.000_{0.105}$	$0.000_{0.000}$	$0.000_{0.014}$	$0.000_{0.003}$	$0.000_{0.078}$	$0.000_{0.064}$	$0.000_{0.047}$	$0.025_{0.107}$	$0.006_{0.087}$	$0.009_{0.088}$	$0.000_{0.000}$	$0.000_{0.000}$	$0.000_{0.000}$
HH	$0.000_{0.000}$	$0.000_{0.050}$	$0.000_{0.034}$	$0.000_{0.010}$	$0.000_{0.000}$	$0.000_{0.000}$	$0.000_{0.000}$	$0.000_{0.016}$	$0.000_{0.001}$	$0.000_{0.000}$	$0.014_{0.071}$	$0.000_{0.055}$	$0.000_{0.026}$	$0.000_{0.000}$	$0.000_{0.000}$	$0.000_{0.000}$

Table 7
Median and IQR of the HV indicator for SparseEA in the nine scenarios.

	Canonical	$EC^{\downarrow}$			$SC^{\downarrow}$			$PF^{\uparrow}$			$PSC^{\uparrow}$			$HF^{\uparrow}$		
		0.1	0.01	0.001	0.1	0.01	0.001	0.1	0.01	0.001	0.1	0.01	0.001	0.1	0.01	0.001
LL	$0.212_{0.051}$	$0.211_{0.053}$	$0.207_{0.051}$	$0.213_{0.052}$	$0.207_{0.044}$	$0.206_{0.053}$	$0.202_{0.066}$	$0.199_{0.061}$	$0.208_{0.061}$	$0.201_{0.048}$	$0.206_{0.069}$	$0.196_{0.050}$	$0.206_{0.061}$	$0.198_{0.053}$	$0.210_{0.061}$	$0.200_{0.064}$
LM	$0.208_{0.069}$	$0.234_{0.052}$	$0.232_{0.063}$	$0.237_{0.067}$	$0.209_{0.060}$	$0.210_{0.052}$	$0.211_{0.050}$	$0.212_{0.057}$	$0.209_{0.040}$	$0.217_{0.049}$	$0.223_{0.051}$	$0.213_{0.037}$	$0.223_{0.052}$	$0.209_{0.051}$	$0.218_{0.049}$	$0.209_{0.057}$
LH	$0.216_{0.055}$	$0.228_{0.063}$	$0.219_{0.058}$	$0.212_{0.067}$	$0.207_{0.057}$	$0.205_{0.054}$	$0.212_{0.049}$	$0.203_{0.057}$	$0.212_{0.051}$	$0.209_{0.054}$	$0.206_{0.055}$	$0.208_{0.054}$	$0.209_{0.045}$	$0.202_{0.066}$	$0.205_{0.054}$	$0.203_{0.057}$
ML	$0.165_{0.045}$	$0.200_{0.079}$	$0.189_{0.046}$	$0.192_{0.063}$	$0.165_{0.051}$	$0.165_{0.044}$	$0.161_{0.038}$	$0.169_{0.050}$	$0.170_{0.042}$	$0.179_{0.056}$	$0.171_{0.043}$	$0.171_{0.046}$	$0.178_{0.046}$	$0.165_{0.050}$	$0.159_{0.057}$	$0.153_{0.046}$
MM	$0.173_{0.041}$	$0.202_{0.043}$	$0.200_{0.042}$	$0.203_{0.043}$	$0.175_{0.047}$	$0.168_{0.035}$	$0.169_{0.025}$	$0.176_{0.053}$	$0.186_{0.042}$	$0.189_{0.035}$	$0.179_{0.053}$	$0.191_{0.035}$	$0.195_{0.038}$	$0.170_{0.039}$	$0.168_{0.044}$	$0.174_{0.030}$
MH	$0.181_{0.040}$	$0.204_{0.046}$	$0.202_{0.045}$	$0.211_{0.059}$	$0.185_{0.055}$	$0.184_{0.040}$	$0.181_{0.052}$	$0.185_{0.043}$	$0.185_{0.051}$	$0.192_{0.056}$	$0.188_{0.036}$	$0.195_{0.051}$	$0.191_{0.048}$	$0.178_{0.055}$	$0.182_{0.059}$	$0.177_{0.040}$
HL	$0.153_{0.036}$	$0.194_{0.056}$	$0.191_{0.039}$	$0.191_{0.049}$	$0.148_{0.041}$	$0.163_{0.043}$	$0.151_{0.034}$	$0.166_{0.052}$	$0.160_{0.053}$	$0.170_{0.050}$	$0.168_{0.056}$	$0.162_{0.049}$	$0.163_{0.047}$	$0.153_{0.046}$	$0.151_{0.044}$	$0.155_{0.051}$
HM	$0.145_{0.042}$	$0.183_{0.054}$	$0.183_{0.038}$	$0.194_{0.047}$	$0.149_{0.053}$	$0.151_{0.047}$	$0.150_{0.047}$	$0.168_{0.042}$	$0.156_{0.054}$	$0.163_{0.039}$	$0.168_{0.040}$	$0.171_{0.046}$	$0.175_{0.046}$	$0.142_{0.042}$	$0.141_{0.050}$	$0.147_{0.043}$
HH	$0.155_{0.040}$	$0.198_{0.055}$	$0.188_{0.053}$	$0.193_{0.042}$	$0.153_{0.039}$	$0.154_{0.047}$	$0.156_{0.058}$	$0.169_{0.038}$	$0.169_{0.036}$	$0.172_{0.036}$	$0.172_{0.037}$	$0.175_{0.044}$	$0.182_{0.058}$	$0.150_{0.042}$	$0.157_{0.041}$	$0.155_{0.047}$

5.2.1. Impact of the problem-specific operators

Let us start by defining our baseline for the comparison. Table 2 includes the median and the Interquartile Range (IQR) of the HV values reached by the canonical MOEAs, that is, those with the default settings described above regarding population size, crossover/mutation operators and rates, etc., and without applying any of the problem-specific operators. A gray background is used in the table cell with the best (highest) HV value.

The starting point is that SMS-EMOA has reached the approximated Pareto fronts with the highest (best) HV indicator values. This is consistent across the nine scenarios and with statistical significance in most cases, as shown in Figure S.9 in the online supplementary material. This is the first relevant finding of this work, as SMS-EMOA has been scarcely used in the context of the CSO problem. To the best of our knowledge, this algorithm has been used in a preliminary study on multi-connectivity in the CSO problem, and no differences have been reported with respect to NSGA-II and MOCell [67].

A second conclusion of the results presented in Table 2 and Fig. 3 is the extremely bad performance of MOEA/D, for which the HV values in each scenario are always zero. This is the effect of the normalization procedure that discards non-dominated solutions out of the limits of the RFP. Fig. 3 graphically shows this fact with the attainment surfaces of the five canonical MOEAs and the RPF for the MM scenario (the same happens in all the other cases, as shown in the figures included in the supplementary material). Note that only those non-dominated solutions having a power consumption below roughly 2 kW (the highest extreme point of the RPF in this objective for this scenario) contribute to the HV value, that is, only NSGA-II, MOCell, SMS-EMOA and SparseEA have a median greater than zero in the row MM of Table 2. The reason for this is that the solutions reached by the hybrid MOEAs with the devised problem-specific operators clearly dominate those of the canonical versions, thus displacing the actual RPF far from the average approximations computed by the canonical versions. After a deep inspection of the MOEA/D implementation used, and available in the jMetal framework (https://github.com/jMetal/jMetal), we can explain this issue in that the evolutionary loop of this algorithm, for which the decomposition-based approach works well for real-coded problems and the Differential Evolution crossover operator, but fails when using binary strings with two-point crossover and bit-flip mutation. Recall that we have kept these common settings across the evolutionary-based MOEAs for comparison purposes. As it can be seen below in Table 6, this happens in most of the results reported by HV involving MOEA/D. As a consequence, from this point onward, we have decided to stop analyzing any results of this algorithm for this quality indicator (removing their contributions to the RPF of each scenario), in order to both reduce the length of the paper and ease its reading. In any case, we would like to point out that problem-specific operators have also improved the search of MOEA/D, as can be seen in the attainment functions reached by the approximated Pareto fronts for the HL scenario, taken as a representative one, in Fig. 4, where the hybrid versions with $EC^{\downarrow}$, $PF^{\uparrow}$, and $PSC^{\uparrow}$ clearly dominate that of the canonical version. The point is that these improvements are not enough to move the approximated Pareto fronts into the limits of the corresponding RPF.

Now, we turn to analyze the actual impact of the five problem-specific operators. Tables 3 to 7 include the median and IQR of the HV values over the 50 runs of NSGA-II, MOCell, SMS-EMOA, MOEA/D and SparseEA for both the canonical and the 15 hybrid versions (five operators applied at three different rates). We will be using the previous names to refer to the canonical MOEAs, and MOEA_{OP}^{rate} to mention a particular hybridization using a given application rate. The tables also use two different gray backgrounds in each row to highlight the best configuration over all settings (darker gray) and the best within a given operator (lighter gray) for each UDN scenario.

The first clear conclusion that can be drawn from all the tables is that hybrid MOEAs have outperformed canonical ones, thus showing

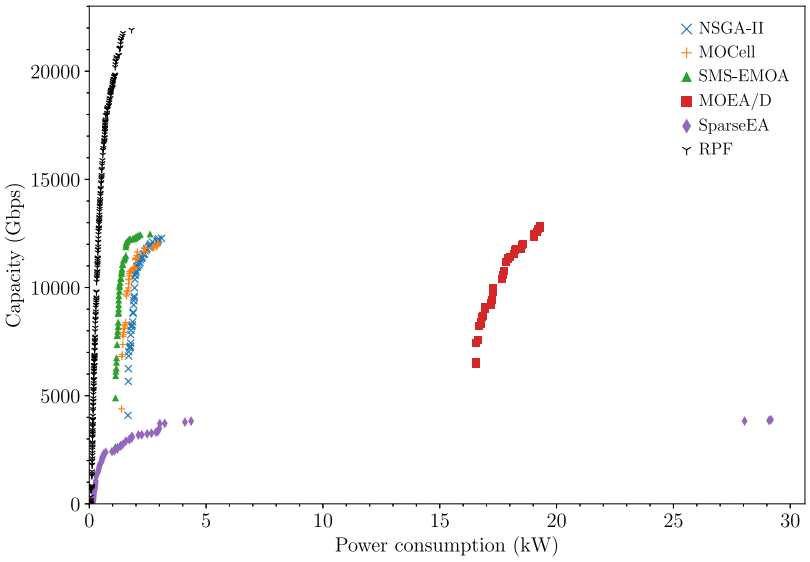

Fig. 3. Attainment functions of the five canonical MOEAs for the MM scenario, and the RPF used in the normalization procedure required to compute the HV indicator.

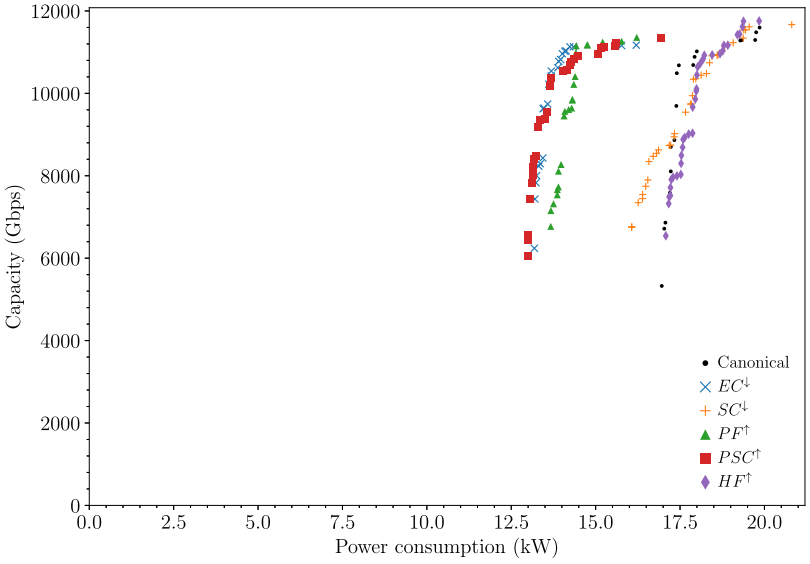

Fig. 4. Attainment functions of both the canonical and hybrid versions of MOEA/D for the HL scenario.

that there is at least one problem-specific operator that has been able to enhance the search capabilities of the algorithms. The dark gray background indicates that the $EC^{\downarrow}$ operator at 0.1 has been able to obtain the best (highest) HV value in most scenarios for NSGA-II (8 out of 9), MOCell (8 out of 9) and SMS-EMOA (6 out of 9), and with statistical significance, as shown in Figures S.10 to S.13.

It is important to remark that most hybrid configurations have enhanced the search of NSGA-II, MOCell and SMS-EMOA, and to a lesser extent that of SparseEA. To better illustrate this fact, we have computed the gap between the HV value of the best application rate for a given operator and the HV value of the canonical MOEA, and have aggregated it over the nine UDN scenarios (LL to HH). The results are shown in Fig. 5, where it can be seen that the HV values have increased substantially, specially in NSGA-II and MOCell, with 0.23 and 0.31, on average, for the five problem-specific operators. Diving a bit deeper into the data reported in this figure, the columns corresponding to the $EC^{\downarrow}$ operator show the maximum gap, that is, the largest increase in the HV value with respect to the canonical version, thus achieving the best-approximated fronts with respect to this indicator. Out of the five devised problem-specific operators, $HF^{\uparrow}$ has provided little-to-no contributions to the search capability of the MOEAs (except for MOCell), even obtaining a negative gap (i.e., the canonical MOEA has outperformed this hybrid version). In fact, averaging the nine scenarios and the three application rates, NSGA-II$_{HF^{\uparrow}}$ has a gap of −0.0013. Despite these results, we will show below, in the next section, that this operator is still useful when combined with others by generating a synergy that enhances the search of MOEAs.

We want to complete our analysis with an operator-wise dimension, that is, how the different combinations of operators and application rates perform. To do so, we computed the average ranking of the HV value for each operator/rate over all the nine UDN scenarios within two different comparison baselines: Table 8 ranks hybrids among the three application rates (that is, the rank is between 1 and 3, which corresponds, respectively, to the best and worst HV value), and Table 9 ranks them among the fifteen hybrids (that is, the rank here ranges between 1 and 15). The first table aims at showing which application rates reached the best (highest) HV value for each operator, whereas the second one compares all the proposed hybrids. The two tables also include a final row that averages the rank over all the four considered

Table 8
Average rank at different application rates of the different hybrid MOEAs for the nine scenarios.

	$EC^{\downarrow}$			$SC^{\downarrow}$			$PF^{\uparrow}$			$PSC^{\uparrow}$			$HF^{\uparrow}$		
	0.1	0.01	0.001	0.1	0.01	0.001	0.1	0.01	0.001	0.1	0.01	0.001	0.1	0.01	0.001
NSGA-II	1.11	1.89	3.00	2.78	1.00	2.22	1.22	1.78	3.00	1.56	1.44	3.00	2.33	2.11	1.56
MOCell	1.11	1.89	3.00	2.78	1.11	1.89	1.33	1.78	2.89	1.56	2.00	2.44	3.00	1.89	1.11
SMS-EMOA	1.44	2.44	2.11	3.00	1.11	1.89	1.67	2.22	2.11	1.22	2.33	2.44	3.00	1.67	1.33
SparseEA	1.56	2.78	1.67	2.11	1.89	2.00	2.56	2.11	1.33	2.44	2.33	1.22	2.22	1.78	2.00
Average	1.31	2.25	2.44	2.67	1.28	2.00	1.69	1.97	2.33	1.69	2.03	2.28	2.64	1.86	1.50

Table 9
Average rank of all the different hybrid MOEAs in all nine scenarios.

	$EC^{\downarrow}$			$SC^{\downarrow}$			$PF^{\uparrow}$			$PSC^{\uparrow}$			$HF^{\uparrow}$		
	0.1	0.01	0.001	0.1	0.01	0.001	0.1	0.01	0.001	0.1	0.01	0.001	0.1	0.01	0.001
NSGA-II	1.22	2.56	7.33	13.22	9.22	11.44	3.22	4.11	8.33	5.11	4.89	9.00	14.00	13.56	12.78
MOCell	1.11	2.44	8.11	14.56	11.78	12.56	5.11	6.11	8.89	4.33	4.78	6.67	12.33	11.00	10.00
SMS-EMOA	1.67	2.89	2.44	12.89	9.89	10.78	5.22	5.56	6.56	5.33	7.33	8.33	15.00	13.33	12.78
SparseEA	1.56	3.11	1.67	11.00	10.67	11.00	9.44	8.22	6.33	7.00	7.33	5.44	13.33	11.11	12.78
Average	1.39	2.75	4.89	12.92	10.39	11.44	5.75	6.00	7.53	5.44	6.08	7.36	13.67	12.25	12.08

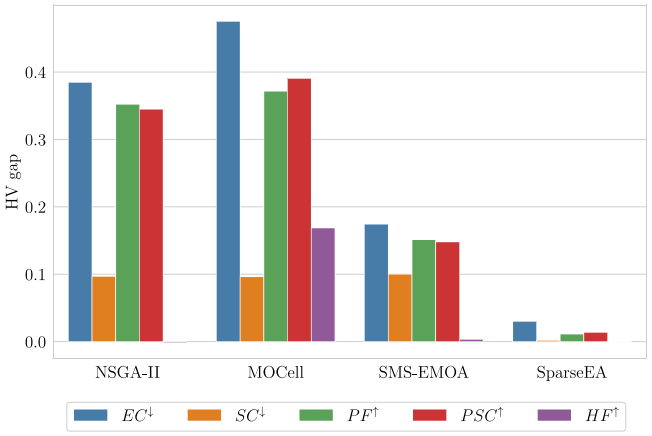

Fig. 5. HV gap between the canonical and the five hybrid MOEAs aggregated over the nine CSO scenarios.

hybrid MOEAs. In order to better support our claims, we have also included in Fig. 6 the attainment functions of both the canonical and the best hybrid versions of the four MOEAs for the scenarios LL, MM and HH, as representative cases with increasing levels of density for UEs and cells (for readability and room constraints, the remaining ones can be found in the supplementary material).

From Table 8, it can be seen that the application rate of 0.1 for $EC^{\downarrow}$ has reported the best ranking (lowest) within the four algorithms separately. The switching off of the empty cells (i.e., not serving any UE) that promotes this problem-specific operator contributes to the search of all the evolutionary loops by introducing many 0's in the tentative solutions (deactivating useless cells) that are managed properly by the genetic operators. The gains in the HV values for NSGA-II, MOCell, and SMS-EMOA are therefore clearly achieved by approximated fronts with non-dominated solutions in the regions of the search space with low power consumption, as can be seen with the blue × in the left-hand side of the subplots in Fig. 6, because a smaller number of cells are operating in the UDN network. Although this is the main effect of the $EC^{\downarrow}$ operator, turning the cells off also allows the removal of interference signals, which also increases SINR and, subsequently, network capacity.

The $SC^{\downarrow}$ operator, which also aims to switch cells off, performs better when applied at a lower rate, 0.01, because it has a stronger effect on the network when applied. In fact, it may deactivate cells even with UEs connected to save energy by sleeping the entire SBS. As a consequence, these UEs have to be reallocated to a different cell, which may cause: (i) that the cell will not to be deactivated on a later iteration, if it was already empty, or (ii) the network capacity is reduced, as the cell bandwidth is shared in a round-robin fashion among all the UEs connected to that cell. Nevertheless, the targeted cells on which the $SC^{\downarrow}$ operator may act are scarce, as it could be difficult to find an SBS in the UDN network with one single cell activated. In any case, the $SC^{\downarrow}$-based hybrid MOEAs can improve on the canonical versions consistently in the nine UDN scenarios. This can be seen in the HV values of the column $SC^{\downarrow}$ in Tables 3 to 7. What the shape of the approximated fronts shows with the attainment functions displayed in Fig. 6 is that in most of the cases for NSGA-II$_{SC^{\downarrow}}$, MOCell$_{SC^{\downarrow}}$ and SMS-EMOA$_{SC^{\downarrow}}$, the canonical versions reach solutions with higher (better) capacity (the two attainments cross towards the right-hand side of the plots). Therefore, the operator is able to enhance the search towards regions with solutions having a lower power consumption in these three classical MOEAs. It has a little-to-no contribution to the search capability of SparseEA.

$PF^{\uparrow}$ and $PSF^{\uparrow}$ report similar results in Table 8: the best rate for NSGA-II, MOCell and SMS-EMOA is 0.1, but the worst for SparseEA. The design goal of these two operators is to switch cells on so that they may serve UEs with higher bandwidth to enhance the second problem objective (capacity), but also with a final call to $EC^{\downarrow}$ (Algorithm 4) to increase energy savings. Therefore, they have reached approximated Pareto fronts with better (higher) values in the network capacity than the $EC^{\downarrow}$-based hybrids, but also with higher power consumption. A clear example is SMS-EMOA and the HH scenario in Fig. 6.i, where the attainment functions with green triangles ($PF^{\uparrow}$) and red squares ($PSC^{\uparrow}$) cross with blue × ($EC^{\downarrow}$) around 1.4 kW. The best application rate of the $HF^{\uparrow}$ operator is 0.001, the smallest possible one, thus showing that, only by itself, the new genetic material introduced in the evolutionary loop is not enough to improve the search of the hybrid MOEAs.

SparseEA deserves special attention, as it is an algorithm specially designed to deal with sparse MOPs. This means that it has concentrated the exploration of the search space in the region with solutions having a very small number of SBSs switched on, thus saving much energy, but, on the contrary, it has not been able to find solutions with comparable values for the capacity objective. As a consequence, SparseEA has also suffered the issue of the HV computation because its approximated fronts are mostly outside the limits of the RPF (this justifies its low HV values in comparison with the other three MOEAs). The last row of Fig. 6 graphically displays this effect. Even though the differences are very tight in the smaller scenario (Fig. 6.j), there is a substantial improvement in the attained fronts when the instances become more complex (higher density). Indeed, the canonical SparseEA is not capable of reaching solutions over about 4000 and 5000 Gbps for the capacity

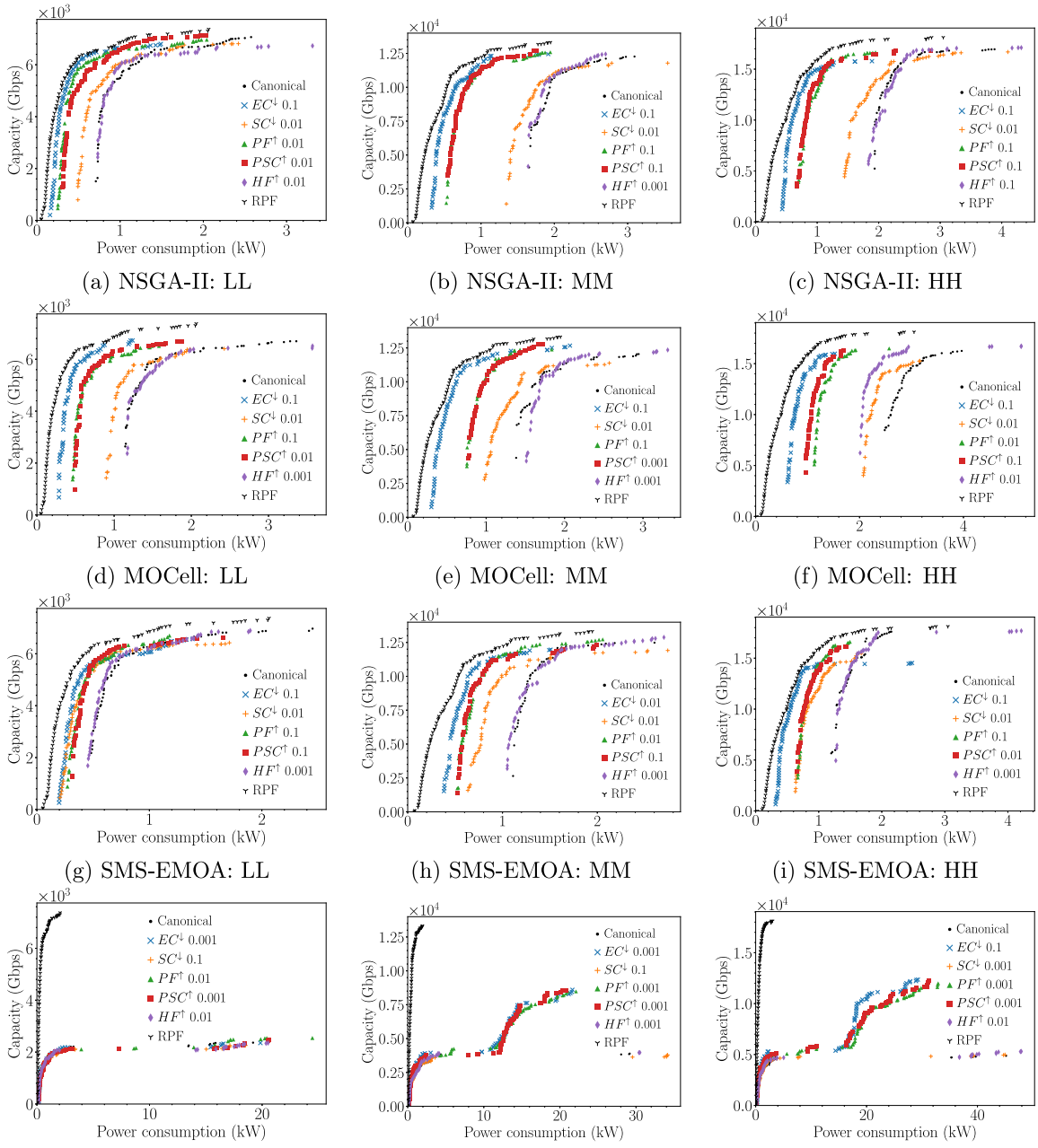

Fig. 6. Attainment functions of both the canonical and hybrid versions of the four MOEAs for three selected UDN scenarios: LL, MM and HH.

objective in the MM and HH scenarios, respectively (Fig. 6.k and Fig. 6.l), but the SparseEA$_{EC^{\downarrow}}$ does, thus showing the advantages of the $EC^{\downarrow}$ problem-specific operator. The point is that the HV computation has not properly captured this information because the extreme value of the power consumption objective in the RPF is fairly low, thus discarding most of the non-dominated solutions above this value.

If we focus on the global ranking among the hybrid versions with $EC^{\downarrow}$, $PF^{\uparrow}$, and $PSC^{\uparrow}$ in Table 9, they have scored the best (lowest) with 3.01, 6.43 and 6.30 average ranks over the three application rates, respectively. The $SC^{\downarrow}$-based hybrid MOEAs can be considered as the fourth out of the five operators with an average rank of 11.58 over the 12.57 of $HF^{\uparrow}$. All these results are supported by the Friedman rank sum test included in the Supplementary material.

We do not want to finish this section without highlighting the actual impact of the improvements in the approximated Pareto fronts within the domain of the CSO problem. As stated above, this work has used a static version of the problem [44], so the objective values can be considered as instantaneous power consumption and network capacity, so even small improvements have a profound impact, specially on the electricity bill over a month/year period for a network operator in their 5G deployments.

5.2.2. *Exploring synergies between operators*

The five problem-specific operators devised in this work try to exploit different features of the CSO problem so that they can be integrated into the search performed by the different MOEAs. Indeed, while two of them promote turning cells off ($EC^{\downarrow}$ and $SC^{\downarrow}$), the other three aim at turning on ($PF^{\uparrow}$, $PSC^{\uparrow}$ and $HF^{\uparrow}$). In the previous section, we have characterized the impact of all of them in an isolated manner, but our hypothesis is that a multi-operator approach in the hybrid MOEAs may generate synergies among them, and improve upon the single-operator ones.

Table 10
Combinations of operators and application rates.

	$EC^{\downarrow}$	$SC^{\downarrow}$	$PSC^{\uparrow}$	$HF^{\uparrow}$
$SYN_1^{\downarrow\uparrow}$	0.100	0.100	0.100	0.010
$SYN_2^{\downarrow\uparrow}$	0.100	0.100	0.010	0.010
$SYN_3^{\downarrow\uparrow}$	0.100	0.100	0.010	0.001
$SYN_4^{\downarrow\uparrow}$	0.100	0.010	0.010	0.010
$SYN_5^{\downarrow\uparrow}$	0.100	0.010	0.001	0.001
$SYN_6^{\downarrow\uparrow}$	0.100	0.001	0.100	0.010
$SYN_7^{\downarrow\uparrow}$	0.100	0.001	0.100	0.001
$SYN_8^{\downarrow\uparrow}$	0.100	0.001	0.010	0.100
$SYN_9^{\downarrow\uparrow}$	0.100	0.001	0.010	0.010
$SYN_{10}^{\downarrow\uparrow}$	0.010	0.001	0.100	0.010
$SYN_{11}^{\downarrow\uparrow}$	0.001	0.100	0.100	0.010
$SYN_{12}^{\downarrow\uparrow}$	0.001	0.100	0.010	0.001
$SYN_{13}^{\downarrow\uparrow}$	0.001	0.010	0.100	0.010
$SYN_{14}^{\downarrow\uparrow}$	0.001	0.010	0.100	0.001

Table 11
Median and IQR of HV for the canonical and both the best single- and multi-operator configurations for NSGA-II in the nine scenarios.

	Canonical	Best single		Best synergy	
LL	$0.521_{0.170}$	$0.766_{0.076}$	$EC_{0.1}^{\downarrow}$	$0.766_{0.074}$	$SYN_9^{\downarrow\uparrow}$
LM	$0.520_{0.185}$	$0.747_{0.071}$	$EC_{0.1}^{\downarrow}$	$0.746_{0.068}$	$SYN_9^{\downarrow\uparrow}$
LH	$0.449_{0.161}$	$0.719_{0.086}$	$EC_{0.1}^{\downarrow}$	$0.712_{0.083}$	$SYN_9^{\downarrow\uparrow}$
ML	$0.271_{0.170}$	$0.739_{0.076}$	$EC_{0.1}^{\downarrow}$	$0.736_{0.077}$	$SYN_6^{\downarrow\uparrow}$
MM	$0.193_{0.231}$	$0.707_{0.070}$	$EC_{0.1}^{\downarrow}$	$0.713_{0.059}$	$SYN_4^{\downarrow\uparrow}$
MH	$0.210_{0.285}$	$0.668_{0.092}$	$EC_{0.1}^{\downarrow}$	$0.677_{0.084}$	$SYN_9^{\downarrow\uparrow}$
HL	$0.365_{0.249}$	$0.720_{0.095}$	$PF_{0.01}^{\uparrow}$	$0.722_{0.092}$	$SYN_7^{\downarrow\uparrow}$
HM	$0.179_{0.265}$	$0.653_{0.093}$	$EC_{0.1}^{\downarrow}$	$0.667_{0.075}$	$SYN_9^{\downarrow\uparrow}$
HH	$0.177_{0.265}$	$0.633_{0.088}$	$EC_{0.1}^{\downarrow}$	$0.643_{0.084}$	$SYN_8^{\downarrow\uparrow}$

The first issue we have to deal with here is the combinatorial explosion of experiments. As a starting point, we have 9 scenarios × 50 seeds × 4 algorithms × 5 operators × 3^3 = 27 possible combinations of the three application rates, which equals 243,000 independent executions. This is obviously not affordable in a reasonable amount of time. To reduce the number of experiments, we have first considered only the LL scenario (the smaller one), and the $PF^{\uparrow}$ operator has been discarded because its results are fairly similar to those of $PSC^{\uparrow}$ (it is more restrictive since it only considers femtocells). From all these combinations, we have ranked them based on the HV value reached for the 50 seeds of the LL scenario, and we have selected those that surpass the median HV value of all the single-operator hybrid MOEAs separately. In total, 14 multi-operator hybrid MOEAs have resulted from this preliminary selection, whose application rates are included in Table 10, and have been used further in the experiments for the eight remaining scenarios (from LM to HH).

Under these experimental conditions, Tables 11 to 14 include the HV value of the approximated Pareto fronts of the canonical and both the best single-operator and best multi-operator hybrid versions of NSGA-II, MOCell, SMS-EMOA, and SparseEA, respectively. The columns aside the HV data link to the configuration that reached that value of Table 10. A gray background has also been used to highlight the best (highest) HV value.

For 20 out of the 36 settings (4 algorithms × 9 scenarios), the multi-operator hybrid MOEAs have been able to improve upon the single-operator setting, thus showing that an effective synergy between operators has been reached. That is, problem-specific operators promoting both switching on and off strategies are useful for improving upon schemes based on a single approach. This synergy has been especially impacted in NSGA-II and MOCell, where $SYN^{\downarrow\uparrow}$ has obtained a higher (better) HV value in 14 out of the 18 comparisons (with statistical significance for most cases in MOCell, as shown in Section 2 of the supplementary material). In order to better illustrate these benefits,

Table 12
Median and IQR of HV for the canonical and both the best single- and multi-operator configurations for MOCell in the nine scenarios.

	Canonical	Best single		Best synergy	
LL	$0.296_{0.188}$	$0.720_{0.073}$	$EC_{0.1}^{\downarrow}$	$0.772_{0.094}$	$SYN_4^{\downarrow\uparrow}$
LM	$0.266_{0.193}$	$0.677_{0.094}$	$EC_{0.1}^{\downarrow}$	$0.729_{0.079}$	$SYN_9^{\downarrow\uparrow}$
LH	$0.258_{0.198}$	$0.623_{0.088}$	$EC_{0.1}^{\downarrow}$	$0.682_{0.073}$	$SYN_9^{\downarrow\uparrow}$
ML	$0.434_{0.212}$	$0.725_{0.100}$	$EC_{0.01}^{\downarrow}$	$0.740_{0.072}$	$SYN_6^{\downarrow\uparrow}$
MM	$0.303_{0.183}$	$0.718_{0.070}$	$EC_{0.1}^{\downarrow}$	$0.696_{0.090}$	$SYN_4^{\downarrow\uparrow}$
MH	$0.036_{0.194}$	$0.591_{0.132}$	$EC_{0.1}^{\downarrow}$	$0.655_{0.076}$	$SYN_9^{\downarrow\uparrow}$
HL	$0.005_{0.199}$	$0.679_{0.103}$	$EC_{0.1}^{\downarrow}$	$0.716_{0.102}$	$SYN_8^{\downarrow\uparrow}$
HM	$0.000_{0.035}$	$0.583_{0.094}$	$EC_{0.1}^{\downarrow}$	$0.643_{0.091}$	$SYN_9^{\downarrow\uparrow}$
HH	$0.000_{0.075}$	$0.559_{0.109}$	$EC_{0.1}^{\downarrow}$	$0.617_{0.072}$	$SYN_9^{\downarrow\uparrow}$

Table 13
Median and IQR of HV for the canonical and both the best single- and multi-operator configurations for SMS-EMOA in the nine scenarios.

	Canonical	Best single		Best synergy	
LL	$0.642_{0.150}$	$0.734_{0.105}$	$EC_{0.1}^{\downarrow}$	$0.747_{0.091}$	$SYN_8^{\downarrow\uparrow}$
LM	$0.594_{0.125}$	$0.721_{0.074}$	$EC_{0.1}^{\downarrow}$	$0.718_{0.089}$	$SYN_{10}^{\downarrow\uparrow}$
LH	$0.556_{0.133}$	$0.685_{0.078}$	$EC_{0.1}^{\downarrow}$	$0.677_{0.082}$	$SYN_{11}^{\downarrow\uparrow}$
ML	$0.519_{0.137}$	$0.725_{0.132}$	$EC_{0.1}^{\downarrow}$	$0.680_{0.128}$	$SYN_7^{\downarrow\uparrow}$
MM	$0.437_{0.141}$	$0.694_{0.086}$	$EC_{0.01}^{\downarrow}$	$0.673_{0.085}$	$SYN_{11}^{\downarrow\uparrow}$
MH	$0.435_{0.191}$	$0.666_{0.095}$	$EC_{0.001}^{\downarrow}$	$0.652_{0.112}$	$SYN_{13}^{\downarrow\uparrow}$
HL	$0.579_{0.161}$	$0.707_{0.086}$	$EC_{0.1}^{\downarrow}$	$0.618_{0.145}$	$SYN_{13}^{\downarrow\uparrow}$
HM	$0.438_{0.160}$	$0.629_{0.101}$	$EC_{0.001}^{\downarrow}$	$0.588_{0.094}$	$SYN_{10}^{\downarrow\uparrow}$
HH	$0.407_{0.204}$	$0.615_{0.089}$	$EC_{0.1}^{\downarrow}$	$0.582_{0.072}$	$SYN_{14}^{\downarrow\uparrow}$

Table 14
Median and IQR of HV for the canonical and both the best single- and multi-operator configurations for SparseEA in the nine scenarios.

	Canonical	Best single		Best synergy	
LL	$0.212_{0.051}$	$0.213_{0.052}$	$EC_{0.001}^{\downarrow}$	$0.237_{0.057}$	$SYN_9^{\downarrow\uparrow}$
LM	$0.208_{0.069}$	$0.237_{0.067}$	$EC_{0.001}^{\downarrow}$	$0.239_{0.060}$	$SYN_9^{\downarrow\uparrow}$
LH	$0.216_{0.055}$	$0.228_{0.063}$	$EC_{0.1}^{\downarrow}$	$0.226_{0.054}$	$SYN_7^{\downarrow\uparrow}$
ML	$0.165_{0.045}$	$0.200_{0.079}$	$EC_{0.1}^{\downarrow}$	$0.209_{0.057}$	$SYN_4^{\downarrow\uparrow}$
MM	$0.173_{0.041}$	$0.203_{0.043}$	$EC_{0.001}^{\downarrow}$	$0.206_{0.043}$	$SYN_4^{\downarrow\uparrow}$
MH	$0.181_{0.040}$	$0.211_{0.059}$	$EC_{0.001}^{\downarrow}$	$0.211_{0.053}$	$SYN_4^{\downarrow\uparrow}$
HL	$0.153_{0.036}$	$0.194_{0.056}$	$EC_{0.1}^{\downarrow}$	$0.208_{0.068}$	$SYN_{10}^{\downarrow\uparrow}$
HM	$0.145_{0.042}$	$0.194_{0.047}$	$EC_{0.001}^{\downarrow}$	$0.191_{0.045}$	$SYN_5^{\downarrow\uparrow}$
HH	$0.155_{0.040}$	$0.198_{0.055}$	$EC_{0.1}^{\downarrow}$	$0.197_{0.070}$	$SYN_5^{\downarrow\uparrow}$

Fig. 7 displays the attainment functions of the best configurations for three scenarios with increasing density levels (i.e., complexity), namely LL, MM and HH. It can be seen that, for these two MOEAs, as long as the density gets larger, the multi-operator hybrids explore better the regions with non-dominated solutions with lower power consumption than that of the single-operator ones, but sacrificing slightly the capacity objective. It is important to note that the best single-operator hybrid is based on $EC^{\downarrow}$, which promotes cell deactivation, but even in this case, the synergy between all can improve upon the power consumption. A problem-side explanation is that an UDN may have more cells switched on, but each consuming less energy (recall that the modeling used for the power consumption is not only based on whether a cell is activated or not, but also on its operating frequency, the traffic load, if it is installed in an SBS with other active cells, etc.). However, SMS-EMOA and SparseEA require further elaboration, as their HV results are again impacted by the normalization process. Indeed, the single-operator hybrid SMS-EMOA has reached the best (highest) value for this indicator in 8 of the 9 UDN scenarios (with very tight differences, actually), but if one analyzes the attainment functions in Figs. 7(g), (h) and (i), it can be seen that the same justification holds as for NSGA-II and MOCell. The only difference is that, on average, the approximated fronts of the SMS-EMOA multi-operator (the + marks) cover solutions with slightly lower network capacity, thus contributing very little to the HV indicator, while the SMS-EMOA single operator (the × marks). In fact, its attainment function seems to be the closest to the RPF in this region of the search space. Finally, by inspecting its attainment surfaces, SparseEA has been clearly the hybrid MOEA that has profited the most with the synergy between the different

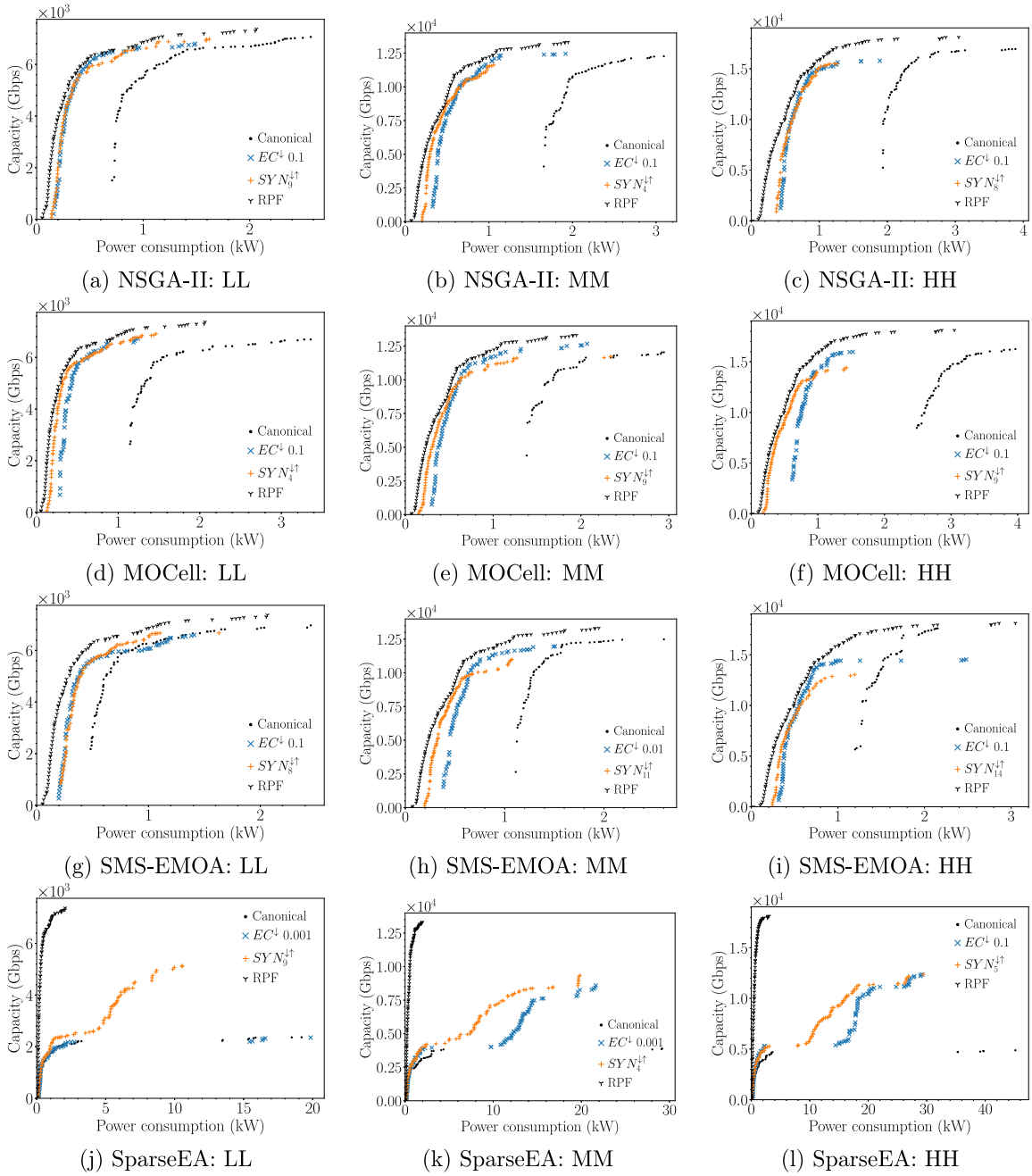

Fig. 7. Attainment functions of the canonical, the best single-operator, and the best multi-operator hybrid MOEAs for three selected UDN scenarios: LL, MM and HH.

problem-specific operators, an important finding not captured by the HV indicator as most of the non-dominated solutions of this MOEA are out of the limit of the RPF. Figs. 7 (j), (k) and (l) clearly show that the median approximated Pareto front of $SYN^{\downarrow\uparrow}$ clearly dominates that of $EC^{\downarrow}$. Being SparseEA an algorithm that seeks solutions with a very small number of 1's (sparse MOP), combining problem-specific operators that not only promote the deactivation, but also the activation of cells has allowed the algorithm to better explore non-dominated solutions with a higher network capacity objective.

6. Conclusions and future work

Ultra-Dense Networks are a key enabler technology for 5G networks, bringing numerous advantages to new small base station deployments. Even so, the massive deployment of small base stations poses a power consumption problem that is being addressed by the research community. This problem has been formulated here as a multi-objective optimization problem, which selectively switches off a subset of small base stations in order to reduce power consumption while maximizing the capacity of network users. In this context, this work proposes the use of hybrid MOEAs to address this issue, incorporating expert knowledge of the problem into the search engine of several algorithms. The results obtained allow us to conclude that hybridization with specific operators, which aim at switching cells on and off, significantly improves the approximated Pareto fronts reached, specially in the power consumption objective. We have also evaluated a multi-operator hybridization, demonstrating that synergies between the different operators can improve upon single-operator-based approaches. Further characterizing these synergies is a limitation of this work. Both all data and the developed software are publicly available

at https://doi.org/10.6084/m9.figshare.21378000 and https://github.com/galeanobra/CSO_Hybrid, respectively.

This work opens up various lines of future work. First, we have worked with five MOEAs that have shown search patterns with different capabilities to explore different regions of the solution space. To exploit these capabilities, we will develop heterogeneous distributed models with several islands. Secondly, we will further seek synergies, not only at a problem-specific operator level, but also with helper objectives that may guide the search towards higher quality solutions. Also, we used for the first time a MOEA designed for sparse problems in the context of the CSO problem. This kind of algorithm is receiving much attention currently in the specialized literature, and deserves a thorough analysis of its performance in the context of our problem. Finally, the modeling of the problem can be evolved to incorporate Cell-Free Massive MIMO technology. This is based on the fact that there are more antennas than users in the scenario, abstracting from the concept "cell", to serve each with multiple antennas. This implies new levels of complexity for the search space, incorporating many more antennas, and changing the allocation strategies between users and base stations.

CRediT authorship contribution statement

Jesús Galeano-Brajones: Software, Investigation, Writing – original draft, Visualization. **Francisco Luna-Valero:** Conceptualization, Methodology, Formal analysis, Investigation, Writing – original draft, Project administration. **Javier Carmona-Murillo:** Validation, Writing – review & editing, Funding acquisition. **Pablo H. Zapata Cano:** Software, Validation, Writing – review & editing. **Juan F. Valenzuela-Valdés:** Conceptualization, Investigation, Writing – review & editing, Funding acquisition.

Declaration of competing interest

The authors declare that they have no known competing financial interests or personal relationships that could have appeared to influence the work reported in this paper.

Data availability

Source code available at https://github.com/galeanobra/CSO_Hybrid and data available at https://doi.org/10.6084/m9.figshare.21378000.

Acknowledgments

This work has been partially funded by the Spanish Ministry of Science and Innovation via grant PID2020-112545RB-C54, by the European Union NextGenerationEU/PRTR under grants TED2021-131699B-I00 and TED2021-129938B-I00 (MCIN/AEI/10.13039/501100011033, FEDER) and the Andalusian PAIDI program with grants A-TIC-608-UGR20, P18.RT.4830, and PYC20-RE-012-UGR. The authors also thank the Supercomputing and Bioinformatics Center of the Universidad de Málaga, for providing its services and the Picasso supercomputer facilities to perform the experiments (http://www.scbi.uma.es/). Funding for open access charge: Universidad de Málaga/CBUA.

Appendix A. Supplementary data

Supplementary material related to this article can be found online at https://doi.org/10.1016/j.swevo.2023.101290.

References

[1] Ericsson, Mobility report, 2022, URL https://www.ericsson.com/49d3a0/assets/local/reports-papers/mobility-report/documents/2022/ericsson-mobility-report-june-2022.pdf.

[2] Cisco, Cisco Annual Internet Report (2018–2023), White Paper, 2020, 2020, URL https://www.cisco.com/c/en/us/solutions/collateral/executive-perspectives/annual-internet-report/white-paper-c11-741490.pdf.

[3] N. Piovesan, A. Fernandez Gambin, M. Miozzo, M. Rossi, P. Dini, Energy sustainable paradigms and methods for future mobile networks: A survey, Comput. Commun. 119 (December 2017) (2018) 101–117, http://dx.doi.org/10.1016/j.comcom.2018.01.005.

[4] J.G. Andrews, S. Buzzi, W. Choi, S.V. Hanly, A. Lozano, A.C.K. Soong, J.C. Zhang, What will 5G be? IEEE J. Sel. Areas Commun. 32 (6) (2014) 1065–1082, http://dx.doi.org/10.1109/JSAC.2014.2328098.

[5] A. Bohli, R. Bouallegue, How to meet increased capacities by future green 5G networks: A survey, IEEE Access 7 (2019) 42220–42237, http://dx.doi.org/10.1109/ACCESS.2019.2907284.

[6] D. Lopez-Perez, M. Ding, H. Claussen, A.H. Jafari, Towards 1 Gbps/UE in cellular systems: Understanding ultra-dense small cell deployments, IEEE Commun. Surv. Tutor. 17 (4) (2015) 2078–2101, http://dx.doi.org/10.1109/COMST.2015.2439636.

[7] M. Kamel, W. Hamouda, A. Youssef, Ultra-dense networks: A survey, IEEE Commun. Surv. Tutor. 18 (4) (2016) 2522–2545, http://dx.doi.org/10.1109/COMST.2016.2571730.

[8] P.K. Agyapong, M. Iwamura, D. Staehle, W. Kiess, A. Benjebbour, Design considerations for a 5G network architecture, IEEE Commun. Mag. 52 (11) (2014) 65–75, http://dx.doi.org/10.1109/MCOM.2014.6957145.

[9] S.A. Busari, K.M.S. Huq, S. Mumtaz, L. Dai, J. Rodriguez, Millimeter-wave massive MIMO communication for future wireless systems: A survey, IEEE Commun. Surv. Tutor. 20 (2) (2018) 836–869, http://dx.doi.org/10.1109/COMST.2017.2787460.

[10] A.L. Swindlehurst, E. Ayanoglu, P. Heydari, F. Capolino, Millimeter-wave massive MIMO: The next wireless revolution? IEEE Commun. Mag. 52 (9) (2014) 56–62, http://dx.doi.org/10.1109/MCOM.2014.6894453.

[11] R.W. Heath, N. González-Prelcic, S. Rangan, W. Roh, A.M. Sayeed, An overview of signal processing techniques for millimeter wave MIMO systems, IEEE J. Sel. Top. Sign. Proces. 10 (3) (2016) 436–453, http://dx.doi.org/10.1109/JSTSP.2016.2523924.

[12] Q.C. Li, H. Niu, A.T. Papathanassiou, G. Wu, 5G network capacity: Key elements and technologies, IEEE Veh. Technol. Mag. 9 (1) (2014) 71–78, http://dx.doi.org/10.1109/MVT.2013.2295070.

[13] X. Ge, S. Tu, G. Mao, C.X. Wang, T. Han, 5G ultra-dense cellular networks, IEEE Wirel. Commun. 23 (1) (2016) 72–79, http://dx.doi.org/10.1109/MWC.2016.7422408.

[14] M. Yao, M.M. Sohul, X. Ma, V. Marojevic, J.H. Reed, Sustainable green networking: exploiting degrees of freedom towards energy-efficient 5G systems, Wirel. Netw. 25 (3) (2019) 951–960, http://dx.doi.org/10.1007/s11276-017-1626-7.

[15] 3GPP, Small Cell Enhancements for E-UTRA and E-UTRAN—Physical Layer Aspects, Tech. Rep., 3rd Generation Partnership Project (3GPP), 2014, URL http://www.3gpp.org/ftp/Specs/html-info/36872.htm.

[16] M. Feng, S. Mao, T. Jiang, Base station ON-OFF switching in 5G wireless networks: Approaches and challenges, IEEE Wirel. Commun. 24 (4) (2017) 46–54, http://dx.doi.org/10.1109/MWC.2017.1600353.

[17] D. Gonzalez G., J. Hamalainen, H. Yanikomeroglu, M. Garcia-Lozano, G. Senarath, A novel multiobjective cell switch-off framework for cellular networks, IEEE Access 4 (2016) 7883–7898.

[18] D. González González, E. Mutafungwa, B. Haile, J. Hämäläinen, H. Poveda, A planning and optimization framework for ultra dense cellular deployments, Mob. Inf. Syst. 2017 (2017) 1–17, http://dx.doi.org/10.1155/2017/9242058.

[19] F. Luna, R. Luque-Baena, J. Martínez, J. Valenzuela-Valdés, P. Padilla, Addressing the 5G cell switch-off problem with a multi-objective cellular genetic algorithm, in: IEEE 5G World Forum, 5GWF 2018 - Conference Proceedings, 2018, pp. 422–426.

[20] P. Zapata-Cano, F. Luna, J. Valenzuela-Valdés, A.M. Mora, P. Padilla, Metaheurísticas híbridas para el problema del apagado de celdas en redes 5G (in spanish), in: XIII Congreso Español En Metaheurísticas Y Algoritmos Evolutivos Y Bioinspirados, MAEB'18, 2018, pp. 665–670.

[21] F. Luna, P. Zapata-Cano, A. Palomares-Caballero, F. Valenzuela-Valdés, A capacity-enhanced local search for the 5G cell switch-off problem, in: Communications in Computer and Information Science, Vol. 1173, CCIS, 2020, pp. 165–178.

[22] K. Deb, A. Pratap, S. Agarwal, T. Meyarivan, A fast and elitist multiobjective genetic algorithm: NSGA-II, IEEE Trans. Evol. Comput. 6 (2) (2002) 182–197.

[23] A.J. Nebro, J.J. Durillo, F. Luna, B. Dorronsoro, E. Alba, Mocell: A cellular genetic algorithm for multiobjective optimization, Int. J. Intell. Syst. 24 (7) (2009) 726–746.

[24] N. Beume, B. Naujoks, M. Emmerich, SMS-EMOA: Multiobjective selection based on dominated hypervolume, European J. Oper. Res. 181 (3) (2007) 1653–1669.

[25] Q. Zhang, H. Li, MOEA/D: A multiobjective evolutionary algorithm based on decomposition, IEEE Trans. Evol. Comput. 11 (6) (2007) 712–731.
[26] Y. Tian, X. Zhang, C. Wang, Y. Jin, An evolutionary algorithm for large-scale sparse multiobjective optimization problems, IEEE Trans. Evol. Comput. 24 (2) (2020) 380–393.
[27] I. Kropp, A.P. Nejadhashemi, K. Deb, Benefits of sparse population sampling in multi-objective evolutionary computing for large-scale sparse optimization problems, Swarm Evol. Comput. 69 (2022) 101025, http://dx.doi.org/10.1016/j.swevo.2021.101025.
[28] E. Zitzler, L. Thiele, Multiobjective evolutionary algorithms: A comparative case study and the strength Pareto approach, IEEE Trans. Evol. Comput. 3 (4) (1999) 257–271.
[29] E. Hossain, V. Bhargava, G. Fettweis, Green Radio Communication Networks, Cambridge University Press, 2012, http://dx.doi.org/10.1017/CBO9781139084284.
[30] G. Miao, G. Song, Energy and Spectrum Efficient Wireless Network Design, Cambridge University Press, 2014.
[31] M. Ismail, M. Shakir, K. Qaraqe, E. Serpedin, Green Heterogeneous Wireless Networks, Wiley, 2016.
[32] S. Buzzi, C.-L. I, T.E. Klein, H.V. Poor, C. Yang, A. Zappone, A survey of energy-efficient techniques for 5G networks and challenges ahead, IEEE J. Sel. Areas Commun. 34 (4) (2016) 697–709, http://dx.doi.org/10.1109/JSAC.2016.2550338.
[33] I.B. Sofi, A. Gupta, A survey on energy efficient 5G green network with a planned multi-tier architecture, J. Netw. Comput. Appl. 118 (2018) 1–28.
[34] M. Usama, M. Erol-Kantarci, A survey on recent trends and open issues in energy efficiency of 5G, Sensors (Switzerland) 19 (14) (2019).
[35] S. Zhang, X. Cai, W. Zhou, Y. Wang, Green 5G enabling technologies: An overview, IET Commun. 13 (2) (2019) 135–143.
[36] P. Karmakar, R. Rajakumar, R. Roy, A survey on energy efficient cellular mobile communication, Wirel. Pers. Commun. 120 (2) (2021) 1475–1500, http://dx.doi.org/10.1007/s11277-021-08520-1.
[37] S. Malathy, P. Jayarajan, H. Ojukwu, F. Qamar, M.N. Hindia, K. Dimyati, K.A. Noordin, I.S. Amiri, A review on energy management issues for future 5G and beyond network, Wirel. Netw. 27 (4) (2021) 2691–2718, http://dx.doi.org/10.1007/s11276-021-02616-z.
[38] A. Mughees, M. Tahir, M.A. Sheikh, A. Ahad, Towards energy efficient 5G networks using machine learning: Taxonomy, research challenges, and future research directions, IEEE Access 8 (2020) 187498–187522, http://dx.doi.org/10.1109/ACCESS.2020.3029903.
[39] I. Chochliouros, M.-A. Kourtis, A. Spiliopoulou, P. Lazaridis, Z. Zaharis, C. Zarakovitis, A. Kourtis, Energy efficiency concerns and trends in future 5G network infrastructures, Energies 14 (17) (2021) http://dx.doi.org/10.3390/en14175392.
[40] O. Alamu, A. Gbenga-Ilori, M. Adelabu, A. Imoize, O. Ladipo, Energy efficiency techniques in ultra-dense wireless heterogeneous networks: An overview and outlook, Eng. Sci. Technol. Int. J. (2020).
[41] G. Premsankar, G. Piao, P.K. Nicholson, M.D. Francesco, D. Lugones, Data-driven energy conservation in cellular networks: A systems approach, IEEE Trans. Netw. Serv. Manag. 18 (3) (2021) 3567–3582, http://dx.doi.org/10.1109/TNSM.2021.3083073.
[42] H.I. Obakhena, A.L. Imoize, F.I. Anyasi, K.V.N. Kavitha, Application of cell-free massive MIMO in 5G and beyond 5G wireless networks: A survey, J. Eng. Appl. Sci. 68 (1) (2021) 13, http://dx.doi.org/10.1186/s44147-021-00014-y.
[43] F. Luna, P.H. Zapata-Cano, J.C. Gonzalez-Macias, J.F. Valenzuela-Valdés, Approaching the cell switch-off problem in 5G ultra-dense networks with dynamic multi-objective optimization, Future Gener. Comput. Syst. 110 (2020) 876–891.
[44] T. Beitelmal, S.S. Szyszkowicz, G. David González, H. Yanikomeroglu, Sector and site switch-off regular patterns for energy saving in cellular networks, IEEE Trans. Wireless Commun. 17 (5) (2018) 2932–2945, http://dx.doi.org/10.1109/TWC.2018.2804397.
[45] W. Lai, C.-S. Shieh, C.-S. Ho, Y.-R. Chen, A clustering-based energy saving scheme for dense small cell networks, IEEE Access 7 (2019) 2880–2893, http://dx.doi.org/10.1109/ACCESS.2018.2886274.
[46] J. Li, H. Wang, X. Wang, Z. Li, Optimized sleep strategy based on clustering in dense heterogeneous networks, Eurasip J. Wirel. Commun. Netw. 2018 (1) (2018) http://dx.doi.org/10.1186/s13638-018-1311-2.
[47] F. Ding, Y. Lu, Z. Pan, D. Zhang, H. Zhu, Performance analysis of an energy-efficient clustering algorithm for coordination networks, Mob. Netw. Appl. 25 (5) (2020) 1632–1643.
[48] A. Hajijamali Arani, M.J. Omidi, A. Mehbodniya, F. Adachi, Minimizing base stations' ON/OFF switchings in self-organizing heterogeneous networks: A distributed satisfactory framework, IEEE Access 5 (2017) 26267–26278, http://dx.doi.org/10.1109/ACCESS.2017.2777914.
[49] M. Dolfi, C. Cavdar, S. Morosi, P. Piunti, J. Zander, E. Del Re, On the trade-off between energy saving and number of switchings in green cellular networks, Trans. Emerg. Telecommun. Technol. 28 (11) (2017) e3193, http://dx.doi.org/10.1002/ett.3193.
[50] F. Ahmed, M. Naeem, W. Ejaz, M. Iqbal, A. Anpalagan, M. Haneef, Energy cooperation with sleep mechanism in renewable energy assisted cellular hetnets, Wirel. Pers. Commun. 116 (1) (2021) 105–124.
[51] Q.-N. Le-The, T. Beitelmal, F. Lagum, S.S. Szyszkowicz, H. Yanikomeroglu, Cell switch-off algorithms for spatially irregular base station deployments, IEEE Wirel. Commun. Lett. 6 (3) (2017) 354–357, http://dx.doi.org/10.1109/LWC.2017.2690677.
[52] F. Lagum, Q.-N. Le-The, T. Beitelmal, S.S. Szyszkowicz, H. Yanikomeroglu, Cell switch-off for networks deployed with variable spatial regularity, IEEE Wirel. Commun. Lett. 6 (2) (2017) 234–237, http://dx.doi.org/10.1109/LWC.2017.2665472.
[53] G. Femenias, N. Lassoued, F. Riera-Palou, Access point switch ON/OFF strategies for green cell-free massive MIMO networking, IEEE Access 8 (2020) 21788–21803.
[54] H. Fourati, R. Maaloul, L. Fourati, M. Jmaiel, An efficient energy-saving scheme using genetic algorithm for 5G heterogeneous networks, IEEE Syst. J. (2022).
[55] A. Salem, S. El-Rabaie, M. Shokair, Energy efficient ultra-dense networks (UDNs) based on joint optimisation evolutionary algorithm, IET Commun. 13 (1) (2019) 99–107.
[56] K. Venkateswararao, P. Swain, Binary-PSO-based energy-efficient small cell deployment in 5g ultra-dense network, J. Supercomput. (2021) 1–22.
[57] D.G. González, J. Hämäläinen, H. Yanikomeroglu, M. García-Lozano, G. Senarath, A novel multiobjective cell switch-off framework for cellular networks, IEEE Access 4 (2016) 7883–7898.
[58] E.-G. Talbi (Ed.), Hybrid Metaheuristics, Studies in Computational Intelligence, vol. 434, Springer Berlin Heidelberg, Berlin, Heidelberg, 2013, http://dx.doi.org/10.1007/978-3-642-30671-6.
[59] Performance limits of multiple-input multiple-output wireless communication systems, in: Space-Time Coding, John Wiley & Sons, Ltd, 2005, pp. 1–47.
[60] J. Son, S. Kim, B. Shim, Energy efficient ultra-dense network using long short-term memory, in: 2020 IEEE Wireless Communications and Networking Conference, WCNC, 2020, pp. 1–6.
[61] C. Von Lücken, B. Barán, C. Brizuela, A survey on multi-objective evolutionary algorithms for many-objective problems, Comput. Optim. Appl. 58 (3) (2014) 707–756.
[62] T. Liu, Z. Wang, M. Wei, A many-objective optimization algorithm using a two-space interactive evolutionary framework, Swarm Evol. Comput. 75 (2022) 101185, http://dx.doi.org/10.1016/j.swevo.2022.101185.
[63] C. Yue, P. Suganthan, J. Liang, B. Qu, K. Yu, Y. Zhu, L. Yan, Differential evolution using improved crowding distance for multimodal multiobjective optimization, Swarm Evol. Comput. 62 (2021) 100849, http://dx.doi.org/10.1016/j.swevo.2021.100849.
[64] Z. Ding, L. Chen, D. Sun, X. Zhang, A multi-stage knowledge-guided evolutionary algorithm for large-scale sparse multi-objective optimization problems, Swarm Evol. Comput. 73 (2022) 101119, http://dx.doi.org/10.1016/j.swevo.2022.101119.
[65] J. Knowles, A summary-attainment-surface plotting method for visualizing the performance of stochastic multiobjective optimizers, in: 5th International Conference on Intelligent Systems Design and Applications, ISDA'05, IEEE, 2005, pp. 552–557.
[66] E. Osaba, E. Villar-Rodriguez, J. Del Ser, A.J. Nebro, D. Molina, A. LaTorre, P.N. Suganthan, C.A. Coello Coello, F. Herrera, A tutorial on the design, experimentation and application of metaheuristic algorithms to real-world optimization problems, Swarm Evol. Comput. 64 (2021) 100888, http://dx.doi.org/10.1016/j.swevo.2021.100888.
[67] A. Quinones-Garcıa, J. Galeano-Brajones, P.H. Zapata-Cano, F. Luna-Valero, J. Carmona-Murillo, J.F. Valenzuela-Valdés, El efecto de la multiconectividad en el problema del apagado selectivo de redes 5G ultradensas [In Spanish], in: XIV Congreso Español De MetaheurísTicas, Algoritmos Evolutivos Y Bioinspirados, 2021, pp. 446–451.